

Evaluating Phasor-Based and Time-Domain Elements for Short Line Applications

Donald D. Fentie
Schweitzer Engineering Laboratories, Inc.

Presented at the
58th Annual Minnesota Power Systems Conference
Saint Paul, Minnesota
November 8–10, 2022

Evaluating Phasor-Based and Time-Domain Elements for Short Line Applications

Donald D. Fentie, *Schweitzer Engineering Laboratories, Inc.*

Abstract—Protective relaying in short line applications challenges engineers to balance the requirements of speed, sensitivity, dependability, and security during faults. Choosing the best protective elements to apply is not always straightforward, and there are more choices available than ever before. In addition to traditional phasor-based protection, new elements and schemes using time-domain incremental quantities and traveling waves (TWs) are now available to provide ultra-high-speed tripping. This paper examines the performance of traditional and ultra-high-speed elements on short line applications. The paper compares the sensitivity and speed of step-distance elements, pilot schemes, and line current differential schemes. Minimum reach considerations for underreaching instantaneous zones are evaluated for step-distance elements in the presence of measurement errors, arc resistance, and system configuration. The paper also evaluates the performance of time-domain elements in weak systems and the effect of TW reflections on TW elements for faults on extremely short lines. Electromagnetic Transients Program (EMTP) simulations are performed on a test system, and the results are played back on TW relays to evaluate performance.

I. INTRODUCTION

A short line is often defined as a line with a source-to-line impedance ratio (SIR) greater than four [1]. Depending on the SIR at each terminal, a line can be *electrically* short at both, one, or neither terminal. Faults on lines with a high SIR challenge protection algorithms, in part, because the measured voltages and currents are small, which can lead to misoperation in the presence of small errors. Traditional instantaneous underreaching distance elements (21Z1) that are applied to short lines have low reach settings that reduce resistive coverage and create concerns about overreach security. This is not limited to mho elements (21M), in which the resistive reach is linked to the reach setting, but also quadrilateral elements (21X), in which the resistive reach setting is practically limited by the impedance reach setting due to the presence of instrument transformer and relay measurement errors.

Solutions that involve communications, such as line current differential (87L) as well as communications-assisted distance and directional overcurrent (67) elements, solve many of the issues of step-distance schemes, but they require dependable communication channel(s) with appropriate bandwidth.

New ultra-high-speed elements that use incremental quantities in a distance-like element (TD21) and directional element (TD32), and a traveling-wave (TW) differential element (TW87) are available as additional choices for protection engineers [2].

This paper examines traditional phasor-based elements, as well as the new time-domain and TW elements and their suitability for short line protection. Section II discusses characteristics of fault impedance due to arc resistance, debris, and tower footing. Section III examines impedance-based protection elements, including 21M and 21X elements. Fault simulations show the performance and suitability of these elements under different types of system conditions on short lines. Section IV covers directional overcurrent performance and sensitivity. Section V lists the pros and cons of line current differential in their application to short lines. Section VI discusses the TD21 element and security features that affect dependability for lines with high SIR. Section VII covers the theory of TD32, application in a permissive scheme, and security features. Section VIII examines TW87 theory and its performance when multiple TW reflections occur within the filter window. It also includes Electromagnetic Transients Program (EMTP) simulations on a short line to analyze the performance for time-domain elements.

II. FAULT IMPEDANCE

Fault impedance includes anything within the path of the fault current, including tower footing, debris, tower structure, and electric arcs. It reduces the resistive coverage of protective relays and is a particular concern on short lines where the fault impedance can be several times the impedance of the line. Fault impedance increases the apparent impedance (affecting distance elements), decreases the operating current for current-based elements, and decreases the magnitude of sequence components that are used in directional elements and other supervisory functions.

A. Tower Footing Resistance

Connecting the tower and ground wire to the earth through the tower footing is an important part of tower construction and design. The resistance between the two is affected by the soil resistivity, ground rods, and counterpoise [1]. Typical values are between 5 and 20 Ω per tower and even higher than 100 Ω in rocky terrains or areas with high soil resistivity [3]. The tower footing resistance is substantially reduced when grounding wires are used, because the ground current is distributed among several towers [1]. Grounding wires and tower footing form ladder networks, as shown in Fig. 1, that can be solved to estimate the effective tower footing impedance [4]. Even in systems with an average footing impedance between 10 and 100 Ω , the effective ground impedance can be as low as 2.8 to 3 Ω when considering the ground wires [5] [6] [7].

Ground fault currents that are caused by insulation flashover or foreign objects pass through the tower footing resistance to complete the return path between the system ground and the earth.

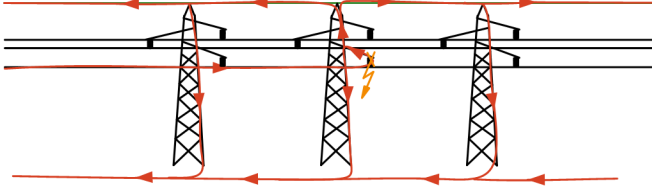


Fig. 1. An overhead ground wire creates a ladder network between towers for a single line-to-ground fault.

B. Objects in Fault Path

The impedance of faults caused by vegetation or debris is unpredictable. One case study in [8] looked at two faults caused by vegetation overgrowth on a 525 kV line. The faults occurred several minutes apart on the same phase, but with very different impedance estimates (350 Ω versus 34 Ω).

The tower structure is also included in the fault current path during an insulator flashover and possibly during phase-to-phase faults. Metallic structures have a negligible impedance, but towers or poles made from nonconductive materials have significant resistance [9].

C. Arc Resistance

An electric arc can form as a multiphase fault between conductors or as a phase-to-ground flashover across a string of insulators. Reference [10] estimates that approximately 80 percent of all faults have an arcing component; therefore, it is important to include it in fault studies. In 1931, electric arc properties were measured and characterized as impedances that are proportional to the arc length L and the inverse of the fault current I , as shown in (1) [11].

$$R_{\text{arc}} \cong \frac{28707 \cdot L}{I^{1.4}} \Omega \quad (1)$$

Research continues to debate and refine the arc resistance calculation to this day [11] [12] [13] [14]. Equation (2) is an alternative arc resistance equation that is commonly used with the voltage gradient constants in Table I. This form of equation is convenient when analyzing impedance elements, because it is easy to convert between arc voltage and arc resistance.

$$R_{\text{arc}} \cong \frac{B \cdot L}{I} \Omega \quad (2)$$

where:

- B is the voltage gradient in volts per meter.
- L is the length of the arc in meters.
- I is the primary fault current in amperes.

TABLE I
TYPICAL VOLTAGE GRADIENTS FOR EQUATION (2)

Method Number	B (V/m)	Ref.
1	1,440	15
2	1,080–1,500	12
3	1,800	16

An arc resistance estimate is found using the constants in Table I and inputting them in (2) and using known parameters for insulator creepage distance and conductor spacing. The arc resistance calculation is approximate if the known fault current is used in the equation. More accurate solutions require iterative techniques, because the equations for fault current and arc resistance are interdependent [12] [17].

There are several properties that separate arc resistance from debris or other objects in the fault current path:

- Infeed from the remote terminal does not magnify the arc resistance measured by the relay, because the arc voltage is relatively constant with fixed arc length regardless of the remote current [4]; however, it can affect the angle of the apparent impedance [5]. This can cause impedance elements to overreach or underreach, as described in Section III.
- Tests confirm that the arc voltage and current are in phase, like a resistor. The arc voltage is quite distorted, but the current is a relatively smooth sinusoid [12].
- The arc length is variable and elongates over time. The length is generally assumed to start as the minimum distance between two objects of different potential and can grow to be two times or more in length [10]. Convection, wind, and electromagnetic attraction all play a role in arc lengthening [17].
- Typical values for arc resistance vary with time, ranging from 1 to 2 Ω for about half a second and possibly peaking above 50 Ω later [3]. There is also a report of the arc impedance decreasing during an arc caused by a wildfire, so it is dependent on the fault conditions [18].

D. Arc Voltage Estimates

Arc voltage (V_{arc}) is estimated using (2) by multiplying the voltage gradient constant in Table I (1,080 to 1,800 V/m) by the arc length. Assuming the arc initially takes the shortest path, the arc length is the distance between two phases for a phase-to-phase fault or the length of the insulator string for a phase-to-ground flashover. The system voltage level plays an important role when designing conductor spacing and insulator creepage distance. Generally, higher voltages require larger spacing between two conductors and between a conductor and the ground. Tower designers must also consider estimated wind speed, pollution levels, tower type (single versus double circuit), tower material, insulation coordination, conductor sag and tension, and more [19] [20].

Table II and Table III show the variation in voltage gradient design in kV/m, as found in different references.

TABLE II
INSULATOR CREEPAGE GRADIENTS

Voltage (kV _{LL})	Voltage Gradient (kV/m)	Notes	Ref.
69	65.3	2-foot insulators	21
Various: 63–245	~26–60	Various tower shapes at different voltage levels	22
Various: 7.5–345	~28.5–68.2	Suspension insulators in outdoor substations using standard 5.75-inch insulators	23
500	78.9	12-foot insulators	21
Transmission (unspecified)	32.3, 40, 50, 62.5	Gradient in order of ascending pollution level (light, medium, heavy, and very heavy)	19

TABLE III
PHASE-TO-PHASE GRADIENTS

Voltage (kV _{LL})	Voltage Gradient (kV/m)	Notes	Ref.
Various: 63–800	~30–67	Various tower shapes at different voltage levels	22
Transmission (unspecified)	32.8	Typical number used in past protection studies	24

There are other standards and references, such as [25], that provide minimum clearance guidance, but these recommendations may be discarded in favor of designs with long-term satisfactory service experience and familiarity in a region [26]. The published clearance data used to calculate the voltage gradients in Table II and Table III suggest that the variability between designs is great, and engineers should use the actual distances in their system for simulations and calculations.

III. IMPEDANCE ELEMENTS

Impedance-based line protective relays use measurements from instrument transformers to calculate an apparent impedance for each fault loop and compare them to one or more operating characteristics. The apparent impedance may not be equal to the true fault impedance, and it can be many times the impedance of a short line. Instantaneous impedance characteristics on short lines are set small to prevent overreach; therefore, resistive coverage is limited. This section describes why there is a practical resistive reach limit, even for 21X, that is related to the reactance reach setting.

This section examines the equations of several impedance methods and their performance on short lines. The system in Fig. 2 is used to simulate the apparent impedance for the different fault types examined in Section II under a variety of system conditions.

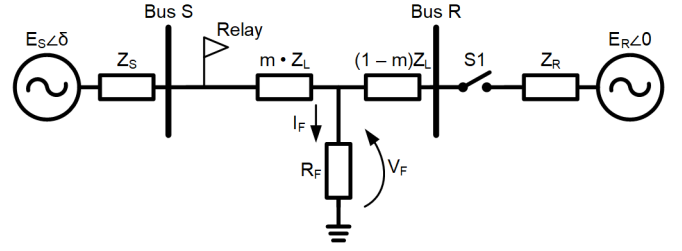


Fig. 2. Two-source system with faulted line.

A. Apparent Impedance Equations for Ground Mho Elements

For an AG fault in Fig. 2, the voltage at the relay V_A is calculated in (3), and apparent impedance Z_{AG_APP} is calculated in (4).

$$V_A = m \cdot Z_{L1} (I_A + k_0 \cdot I_R) + V_{AF} \quad (3)$$

where:

k_0 is the compensation factor equal to $(Z_{L0} - Z_{L1}) / 3Z_{L1}$.

I_R is the residual current equal to $I_A + I_B + I_C$.

V_{AF} is the fault voltage for the AG fault.

$$Z_{AG_APP} = \frac{V_A}{I_A + k_0 \cdot I_R} = m \cdot Z_{L1} + \frac{V_{AF}}{I_A + k_0 \cdot I_R} \quad (4)$$

Therefore, the apparent impedance in the fault Z_{F_APP} is shown in (5).

$$Z_{F_APP} = \frac{V_{AF}}{I_A + k_0 \cdot I_R} = \frac{I_F \cdot R_{AF}}{I_A + k_0 \cdot I_R} \quad (5)$$

where:

R_{AF} is the fault impedance between Phase A and the ground.

Consider an AG fault at $m = 0.5$ pu on the system in Fig. 2 when Switch S1 is open. The system is radial with no load flow. Therefore $I_F = I_R = I_A$, and the apparent impedance Z_{F_APP} becomes $R_{AF} / (1 + k_0)$. If the same fault is applied with S1 closed (looped system) and the source voltages and impedances are identical, then the fault current from each source is equal ($m = 0.5$ pu). The voltage across the fault V_{AF} is $2 \cdot R_{AF} \cdot I_A$, and Z_{F_APP} is twice as large in the looped system compared to the radial system.

1) Ground Quadrilateral Equations

In this section, the mho and quadrilateral elements are plotted on a different impedance plane than the apparent impedance plane. The impedance points for the quadrilateral are calculated by extracting the reactance and estimated fault resistance from the applied signals, as shown in the following equations. The impedance is compared against the quadrilateral characteristic. One ground quadrilateral design calculates the resistance separate from the line impedance [27] [28]. Equation (3) is rewritten with fault impedance R_{AF} in (6).

$$V_A = m \cdot Z_{L1} (I_A + k_0 \cdot I_R) + R_{AF} \cdot I_F \quad (6)$$

R_{AF} is solved by multiplying each term in (6) by $(m \cdot Z_{L1} (I_A + k_0 \cdot I_R))^*$ and then taking the imaginary of each term. Equation (7) is an estimate of a resistive fault impedance.

$$R_{AF} = \frac{\text{Im}(V_A (m \cdot Z_{L1} (I_A + k_0 \cdot I_R))^*)}{\text{Im}(I_F (m \cdot Z_{L1} (I_A + k_0 \cdot I_R))^*)} \quad (7)$$

The true fault current I_F is unknown to the local relay in a looped system (assuming data are not transmitted from the relay at the remote bus). Equation (8) eliminates load flow effects by removing the positive-sequence current I_1 from I_F .

$$I_F = 1.5(I_2 + I_0) \quad (8)$$

A similar approach is used to calculate the impedance reach $m \cdot |Z_{L1}|$ along the line angle [29]. Solving (6) for apparent impedance $Z_{AG_{APP}}$ is shown in (9).

$$Z_{AG_{APP}} = m \cdot Z_{L1} + R_{AF} \cdot \frac{I_F}{I_A + k_0 \cdot I_R} \quad (9)$$

The reactance line is tilted by an equivalent angle of $\arg [I_F / (I_A + k_0 \cdot I_R)]$ so that the element does not overreach or underreach when load flow is present during a resistive fault. This is achieved by choosing a polarizing current I_{POL} with the same angle as I_F in a homogeneous system (such as I_2 or I_0). Any extra tilt caused by system nonhomogeneity is provided by a user tilt setting T .

Each term in (6) is multiplied by $(I_{POL} \cdot e^{jT})^*$, where I_{POL} is I_2 or I_0 . The term that contains fault resistance R_{AF} becomes zero when you take the imaginary component of both sides of the equation and then calculate the impedance of the quadrilateral along the line angle Z_{XAG} , as shown in (10).

$$Z_{XAG} = m \cdot |Z_{L1}| = \frac{\text{Im}(V_A (I_{POL} \cdot e^{jT})^*)}{\text{Im}((1 \angle ZIANG)(I_A + k_0 \cdot I_R)(I_{POL} \cdot e^{jT})^*)} \quad (10)$$

where:

$ZIANG$ is the positive-sequence angle of the line.

Equations (7) and (10) form the real and imaginary components of a complex impedance that is compared against the resistive reach and impedance reach settings, as shown in Fig. 3.

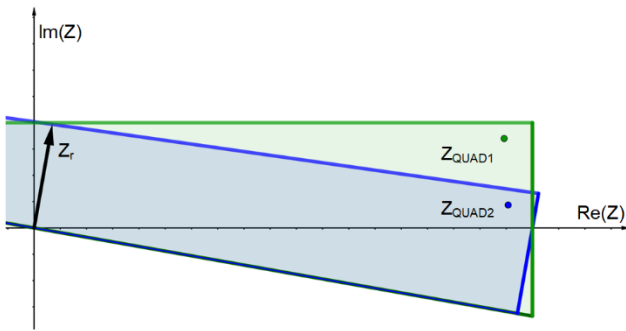


Fig. 3. Z_{QUAD1} is calculated using (7) and (10), and it is compared against the resistive and impedance reach (green). Z_{QUAD2} is the equivalent point on the tilted quadrilateral characteristic (blue).

Equations (7) and (10) are convenient, because they account for blinder tilting and can be directly compared to the scalar

reach setting and the resistance setting. Consider an AG fault at $m = 0.5$ on the system in Fig. 2 when Switch S1 is open. In this case, R_{AF} is equal to the true fault impedance. If S1 is closed, the voltage across the fault impedance doubles; therefore, the relay will calculate fault resistance as twice the R_{AF} .

2) Apparent Impedance Equations for Phase Mho Elements

The loop voltage measured at the relay for a BC fault is shown in (11).

$$V_{BC} = m \cdot Z_{L1} \cdot I_{BC} + V_{BCF} \quad (11)$$

where:

$V_{BCF} = V_{BF} - V_{CF}$, which represents the voltage drop across the fault impedance.

Consider a BC fault at $m = 0.5$ on the system in Fig. 2 when Switch S1 is open (radial system, $I_B = -I_C$). From (12), the apparent fault impedance $Z_{F_{APP}}$ is half the true fault impedance since the phase current I_{BC} can be written as $2 \cdot I_B$ for a phase-to-phase fault.

$$Z_{BC_{APP}} = \frac{V_{BC}}{I_{BC}} = m \cdot Z_{L1} + \frac{V_{BCF}}{I_{BC}} \quad (12)$$

If the same fault is applied with S1 closed, the system is now looped, and the fault voltage V_{BCF} is affected by infeed from the remote source. The fault in the example is at the midpoint of the line ($m = 0.5$) with no load flow, and the source impedances and strength at each end of the line are equal. Therefore, the fault current supplied from each end is equal, and the voltage across the fault impedance V_{BCF} is twice as large as for the radial system. In this example, $Z_{F_{APP}}$ is equal to the true fault impedance when V_{BCF} is divided by I_{BC} .

3) Phase Quadrilateral Equations

Similar to the ground quadrilateral section, the reactance and estimated fault resistance are calculated for the phase quadrilateral element. First, write (11) in terms of fault resistance and fault current, as shown in (13).

$$V_{BC} = m \cdot Z_{L1} \cdot I_{BC} + R_{BCF} \cdot I_F \quad (13)$$

where:

R_{BCF} is the true fault impedance between Phases B and C.

The line impedance term in (13) is eliminated by multiplying all terms by the conjugate of the appropriate polarizing quantity I_{POL} and taking the imaginary component of each term. For a BC fault, the polarizing current $I_{POL} = j \cdot I_2 \cdot (1 \angle ZIANG)$ has the same angle as I_{BC} assuming no load flow, and the resistance is calculated in (14).

$$R_{BCF} = \frac{\text{Im}(V_{BC} \cdot I_{POL}^*)}{\text{Im}(I_{BC} \cdot I_{POL}^*)} \quad (14)$$

The impedance reach along the line angle, Z_{XBC} , is solved similarly using $I_{POL} = j \cdot I_2 \cdot e^{jT}$, where T is a user setting that applies extra tilt to the reactance line, as shown in (15).

$$Z_{XBC} = m \cdot |Z_{L1}| = \frac{\text{Im}(V_{BC} \cdot I_{POL}^*)}{\text{Im}(I_{BC} \cdot (1 \angle Z_{L1}) \cdot I_{POL}^*)} \quad (15)$$

The polarizing quantities used in (14) and (15) cause the reactance and resistance blinders to tilt and prevent the apparent impedance calculated in (12) from underreaching or overreaching depending on the direction of the load flow. Equations (14) and (15) can also be compared directly to the phase reactive and resistive reach settings, respectively.

For three-phase faults, a polarizing quantity using positive-sequence current is typically used instead of a polarizing quantity using negative-sequence current. One design shrinks the resistive reach to 25 percent of the setting for three-phase faults to reduce the overreaching effects of load flow [30]. This design also modifies the angles of the other blinders, as shown in Fig. 4.

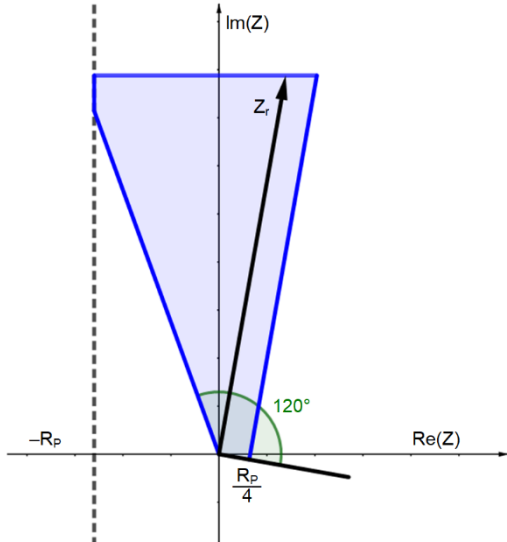


Fig. 4. One type of phase quadrilateral characteristic during three-phase faults. (R_p is the phase resistive reach setting.)

B. SIR Considerations

IEEE Std C37.113, *IEEE Guide for Protective Relay Applications to Transmission Lines* defines a short line as a line with an SIR greater than four [1]. This section explores several impacts of a higher SIR, including mho expansion, distance element operating speed, sensitivity, and capacitor voltage transformer (CVT) transients. The impedance equations from the previous subsection are used in the system shown in Fig. 2 under a variety of SIR conditions.

1) Mho Expansion

Mho elements in modern microprocessor relays use a polarizing voltage with memory to remain dependable and secure for close-in faults [28] [31]. This causes the mho circle to expand for faults in the direction of the element reach and increases resistive coverage. The size of the expansion is directly proportional to the SIR since the dynamic mho circle includes the source impedance vector Z_s , as shown in Fig. 5.

Memory voltage begins to decay after the initial expansion, and this causes the dynamic mho circle to shrink over time until it reaches a steady state. The steady state size of the characteristic depends on the type of polarization used, system parameters, and the type of fault applied [32]. In Fig. 5, Z_r is the reach setting, Z is the measured apparent impedance, Z_p is the polarizing impedance, and Z_s is the source impedance.

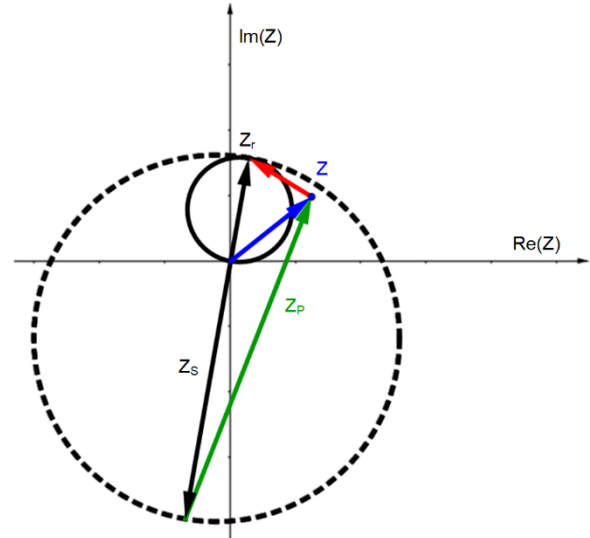


Fig. 5. Phase mho with dynamic (dashed) and self-polarized (solid) circles.

Fig. 6 shows the mho expansion for faults on the line in Fig. 2 with S1 closed under varying local SIR values and constant fault resistance. As the local source impedance increases (and therefore, the SIR increases), the dynamic mho circle becomes larger. The resistive coverage appears to improve with the larger characteristic, but the infeed from the remote terminal magnifies the apparent impedance Z , moving it outside the dynamic mho circle.

Fig. 6a

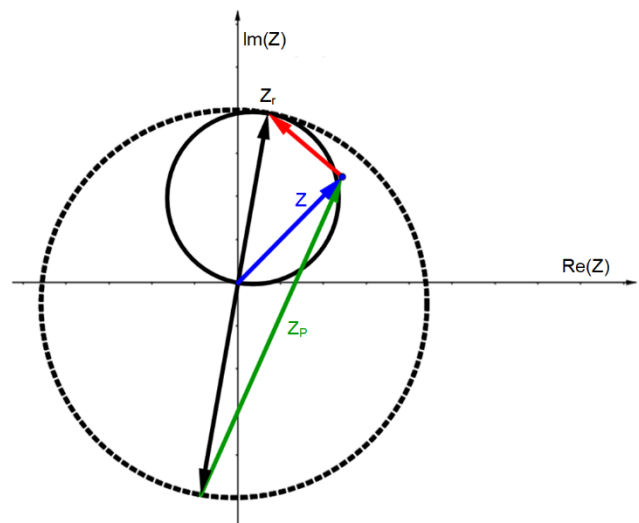


Fig. 6b

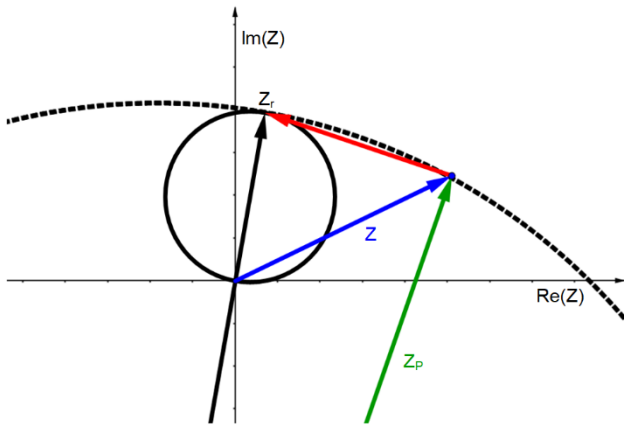


Fig. 6c

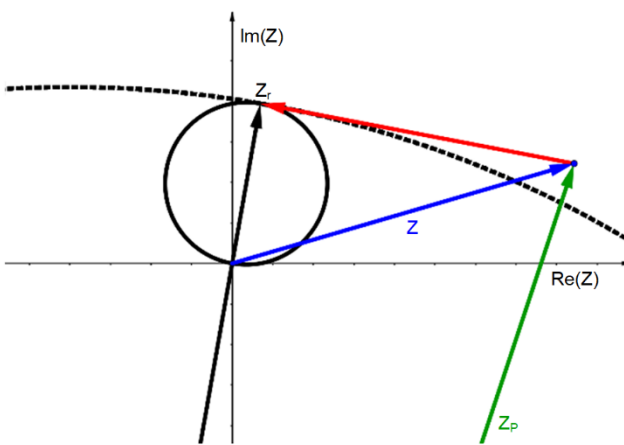


Fig. 6. BC fault with dynamic mho circle (dashed) for different local SIRs, including the remote SIR = 1 (fixed) and local SIR: (a) SIR = 1, (b) SIR = 5, and (c) SIR = 10.

2) Fault Impedance Versus Arc Resistance

The apparent impedance calculated for faults involving debris is magnified by the remote infeed current. Assuming equal source voltage in the two-source system of Fig. 2, the ratio of SIR_{LOCAL} to SIR_{REMOTE} and fault location determine the proportion of fault current contribution from each end. If the ratio increases, the remote source supplies a greater portion of the fault current and contributes to a greater portion of the voltage drop across the fault impedance. The infeed from the remote terminal increases the apparent impedance calculated by the relay at the local terminal.

For faults that contain only an electric arc, the infeed does not change the magnitude of the apparent impedance seen by the relay, because the arc voltage inferred from (2) depends on the length of the arc and the voltage gradient, but not the contribution of remote current. The relay measures a higher apparent impedance magnitude for arc resistance with a larger local SIR, because the fault current contribution from the local terminal decreases. The arc voltage can exceed the voltage drop across the line for higher levels of SIR at the local terminal, as shown in Fig. 7. Therefore, arc resistance can be significant in short line applications and should be considered when

evaluating impedance element dependability, sensitivity, and security [33].

Fig. 7a

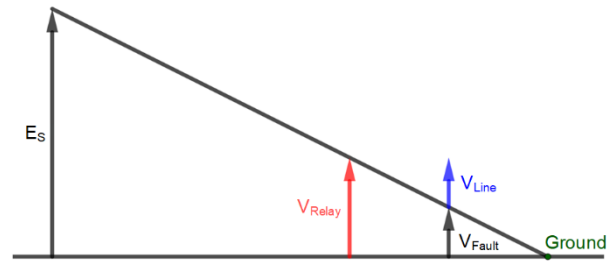


Fig. 7b

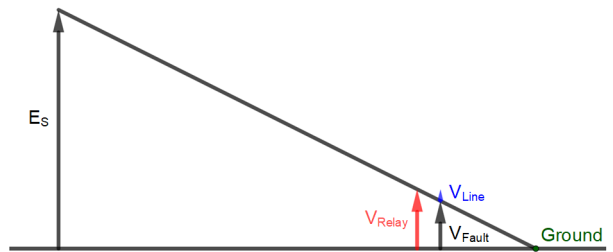


Fig. 7. Voltage profile during a ground fault with pure arc resistance for a system with (a) lower SIR and (b) higher SIR.

3) Speed

Equation (16) defines the mho element as the torque product between the conjugate of the polarizing voltage, V_{POL} , and the operate quantity $Z_r \cdot I - V$

where:

Z_r is the relay reach.

I is the fault loop current.

V is the measured fault loop voltage.

$$\text{RE}((Z_r \cdot I - V) V_{POL}^*) > 0 \quad (16)$$

In electromechanical relays, the greater the torque product in (16), the faster the operation. A lower torque value results in slower operation, which occurs when the fault is near the reach point or when the fault occurs in a weak system. Since microprocessor relays do not produce a physical torque, the relay designers must apply filtering, security delays, and other measures to achieve low transient overreach. This also results in operate speed curves that depict slower performance for higher levels of SIR and faults closer to the reach point. Therefore, even though torque does not directly apply to microprocessor relays, it can still be thought of in a similar way.

Consider a fault applied to Fig. 2 with fixed fault location m , line impedance, and relay reach point Z_r . Increasing the source impedance Z_s increases the SIR and reduces the measured voltage at the relay V and the measured loop current I . Lower measured voltage and current reduces the torque product and slows down the operation of the relay. Fig. 8 shows how the SIR affects operating speed of a digital relay for faults applied at different points along the line [34]. The operating time curve is flat when the SIR is high, because most of the voltage drop occurs across the source impedance. Therefore, faults at different locations on the line produce smaller changes in the

voltage and current measured by the relay, and the torque product produced by (16) is within a narrow range.

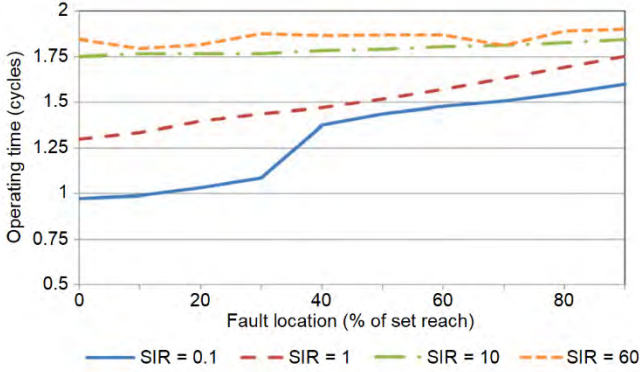


Fig. 8. Operating time versus fault location for distance elements with different SIRs [34].

4) Limits to Sensitivity

Reference [14] describes protection accuracy issues in systems with a high SIR, particularly when using CVTs. Consider bolted faults applied to the system in Fig. 2 for a homogeneous system with a varying SIR. Table IV shows that the difference in voltage measured by the relay for a fault at the reach point and a fault at the remote bus is dependent on the SIR.

TABLE IV
MEASURED VOLTAGE BASED ON FAULT LOCATION*

Fault Location	SIR	Measured Relay Voltage (V Secondary)
Reach point	10	4.96
Remote bus	10	6.09
Reach point	40	1.31
Remote bus	40	1.63

* Fault location is based on bolted fault with reach Z_r set to 0.8 pu of line. Source voltage E_s is fixed at 67 V secondary.

In the system where $SIR = 10$, the voltage difference is greater than 1 V, but in the system with $SIR = 40$, the voltage difference is about one-third of a volt. Any errors in the measurement from the instrument transformers or relay can have a big impact on the decision to trip or restrain. One utility requires a minimum difference of 1 V secondary between faults at the reach point and remote bus. Otherwise, the reach setting is pulled back [35]. This can also be represented as an overcurrent threshold, as described in Section VI.

Published relay specifications show that relay error is greater for higher SIRs, but the typical transient error is less than 5 percent [36] [37], and transient CVT errors are typically less than 10 percent in the first cycle after a fault [36]. Adding these errors quadratically yields a composite error θ_e of 11.2 percent. As shown in Fig. 9, this error can exceed the difference in voltage measured by the relay for a fault at the reach point and remote bus (V_{Diff}). In this case, the relay might overreach. Specific solutions to overcome CVT transients are discussed in the next subsection, but this solves only part of the sensitivity issue.

Fig. 9a

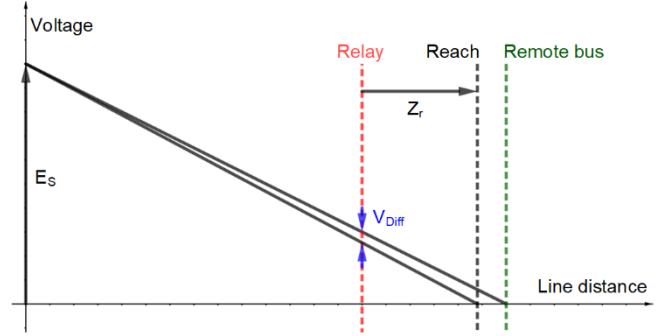


Fig. 9b

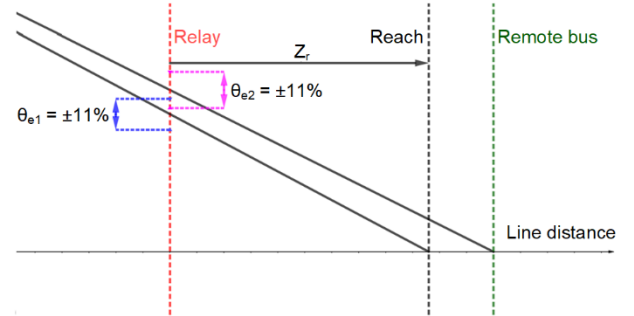


Fig. 9. Faults occur at the remote bus and reach point for the short line. These figures show (a) the voltage profile of the entire line and (b) the zoomed-in voltage profile near the relay and fault point.

Another source of error that primarily affects ground distance elements is the ground potential rise (GPR). The GPR occurs when the substation ground potential is higher than the earth potential at the remote end of the line (i.e., remote earth potential) due to zero-sequence current sinking into the substation ground [38]. This causes the relay to measure low voltage at the voltage transformers (VTs) and the ground distance elements to overreach. Phase elements are not affected, because the phase-to-phase voltage calculations cancel out zero-sequence quantities. Ground distance elements in substations with high levels of GPR should be considered carefully.

5) CVT Transients

CVTs are commonly used with protective relays today and are known to have a poor transient response in systems with high SIRs. Reference [39] describes two different types of CVT technology: one that uses active ferroresonance-suppression circuits (AFSCs) and another that uses passive ferroresonance-suppression circuits (PFSCs). The transient response from a CVT that occurs within 1 to 2 cycles of a fault can significantly reduce the voltage magnitude calculated by the relay after passing through the relay digital filters [39]. This jeopardizes the security of underreaching instantaneous impedance elements, because the impedance trajectory moves closer toward the origin on the impedance plane (relay location). CVTs with PFSCs are expected to perform properly for up to 80 percent reach for systems with SIRs of 30; but CVTs with AFSCs have a much more pronounced transient,

and without CVT transient detection in the relay, a secure reach setting drops sharply as the SIR increases [40].

CVT detection logic is built into most modern relays to provide additional security through one of several methods: an additional delay to ride through the transient, special filtering to remove the transient, smoothing detection logic to determine when the transient has subsided, or all three [37] [39]. On short lines when CVTs are present, CVT transient logic should be enabled if available, or an extra time delay can be added to the Zone 1 element. Another option is to disable the Zone 1 element completely and explore alternative forms of line protection, such as using a pilot scheme.

For relays without transient detection logic, [39] provides typical maximum reach plots for distance elements where CVTs are applied. The recommended pullback for distance elements that use AFSC CVTs is so large that users may not want to apply instantaneous distance elements on short lines without transient detection. Since the reach is often set very small for instantaneous zones on short lines, further reducing the reach may not be an option. Recent literature challenges the need to pull back the reach in modern relays with CVT logic enabled, but it remains a common modern practice [35].

C. Quadrilateral Resistive Reach Considerations

Quadrilateral elements have an advantage over mho elements, because the resistive reach setting is set independently from the reactive reach. However, the quadrilateral resistive reach setting cannot be set infinitely large, and it also should not be set to the maximum allowable setting in the relay for short lines. The resistive reach has a practical limit because of small errors θ_e inherent to the system, instrument transformers, and relay measurements. As shown in Fig. 10, θ_e can cause a quadrilateral element with high resistive reach to overreach for high-impedance faults at the remote bus. Maximum loading should always be considered and load encroachment characteristics used when appropriate.

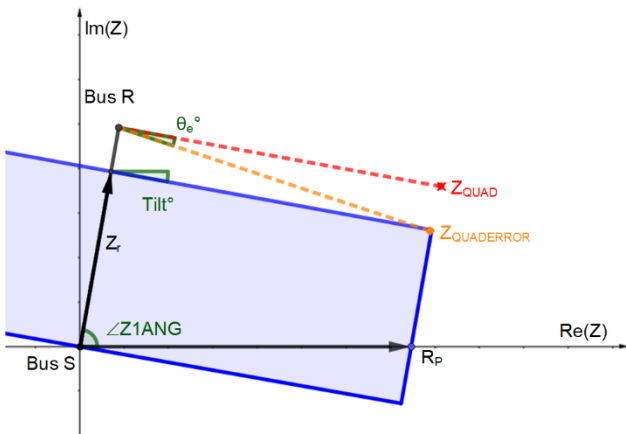


Fig. 10. Quadrilateral overreach due to measurement errors.

Reference [24] derives the maximum resistive reach, R_{MAX} , as shown in (17).

$$R_{MAX} = \left(\frac{\sin(\theta_e + Z1ANG)}{\sin(\theta_e)} (1 - Z_{rpu}) |Z_{L1}| \right) \quad (17)$$

where:

Z_{rpu} is the relay reach in pu.

$Z1ANG$ is the positive-sequence line angle in degrees.

Z_{L1} is the positive-sequence line impedance in Ω secondary.

θ_e is the composite measurement errors in degrees.

The variable θ_e is typically 2 to 3 degrees using conservative estimates for current transformer (CT) angle errors (1 degree), VT angle errors (2 degrees), and relay measurement angle errors (0.2 degrees) [9] [41]. From (17), the maximum safe resistive reach is directly proportional to Z_{rpu} . For example, consider a short line where $Z_{L1} = 0.1 \Omega$ secondary, $Z1ANG = 80$ degrees, $\theta_e = 3$ degrees, and reach $Z_{rpu} = 0.8$ pu; R_{MAX} is calculated as 0.379Ω .

D. Is Step Distance Adequate?

This section explores if step-distance protection is adequate for short lines. It compares mho and quadrilateral performance in various simulations and discusses whether or not there is a rule of thumb for a minimum reach setting.

1) Minimum Allowable Relay Reach Setting

Electromechanical distance relays have a minimum allowable reach setting that is much greater than modern microprocessor relays. For example, a popular older electromechanical relay has a minimum pickup of 0.2Ω secondary [42], and it also requires a significant fault current to operate at low tap settings. In comparison, a modern microprocessor relay with a 5 A channel has a minimum reach setting of 0.05Ω secondary [37]. Modern relays often supervise distance elements with minimum current thresholds, such as fault detectors that are embedded into the directional elements [43].

If an instantaneous impedance element is set within the allowable relay settings range, it does not necessarily mean that it is suitable for application on a short line, as explained in the next subsection. Relay underreach or overreach depends on many factors, such as the level of arc resistance, fault impedance, infeed, SIR, mutual coupling, and errors from the relay and instrument transformers.

2) Impedance Simulations

Consider Fig. 2 with Switch S1 closed. Faults are applied at various locations on the line under different system conditions in Fig. 11 to Fig. 14. The apparent impedance is plotted for the mho element using (4) and (12), and the dynamic properties of the mho are also simulated assuming positive-sequence polarization [44]. The quadrilateral elements are calculated using (7), (10), (14), and (15). Then the equivalent point is plotted on the tilted quadrilateral characteristic for a visual representation. In each simulation, the quadrilateral reach is set, per (17), with $\theta_e = 3$ degrees. Simulations with arc resistance

use 1,800 V/m for a conservative voltage gradient from Table I. All dynamic mho circles are shown at a steady state.

Figures in this section represent faults simulated on a 500 kV line with a CT ratio of 400:1 and potential transformer (PT) ratio of 4500:1, unless otherwise stated. Insulator creepage distance is 3.66 m (12 ft) and 9.96 m between conductors.

In Fig. 11, the fault impedance is pure arc resistance for an AG fault (Fig. 11a) and a BC fault (Fig. 11b). The impedance loci are shown for minimum arc length or 1 pu (3.66 m) and 3 pu (10.98 m) to account for arc lengthening. The impedance is plotted as the fault is moved down the line from the local bus ($m = 0$) to 80 percent of the line ($m = 0.8$).

Fig. 11a

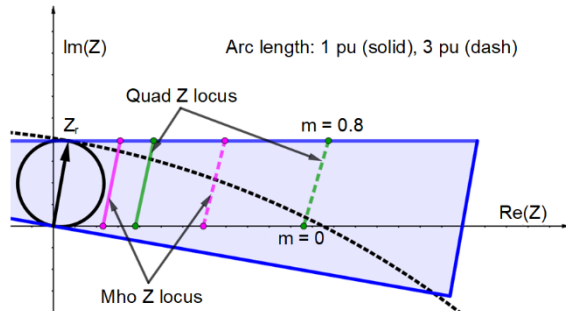


Fig. 11b

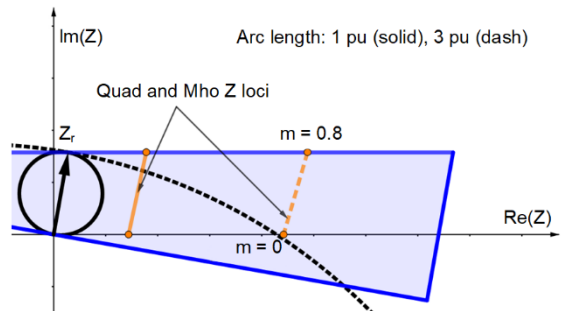


Fig. 11. Arc resistance impedance loci from 0 percent of the line to 80 percent (reach point) with no load flow, with an SIR of 20, (a) an AG fault with 3.66 m (12 ft) insulators, and (b) BC fault with 9.96 m conductor spacing. The dashed curve represents mho expansion.

Fig. 11 shows that the quadrilateral element has better resistive coverage than the mho, even when considering dynamic mho expansion. The mho and quadrilateral loci do not plot in the same location on the AG plot, because the ground mho calculations for R_F divide by $(1 + k_0)$, whereas the ground quadrilateral attempts to calculate the exact R_F . The apparent impedance seen by the relay due to arc resistance is proportional to the SIR at the local terminal. Two lines of different length and impedance can measure the same apparent arc resistance if they have the same SIR, but it is more likely that a geometrically short line has a higher SIR than a long line.

Fig. 12 shows the AG fault loci with the same parameters as Fig. 11, except with a negative 30-degree load angle (import power). The polarization of the quadrilateral tilts the top of the reactance blinder, as discussed in Section III.A, and this helps maintain dependability. For export power scenarios, the quadrilateral tilts the top of the reactance blinder downward, and this helps prevent overreach. The dynamic mho

characteristic also tilts based on the load flow since the load angle affects the angle of the polarizing voltage, and therefore, the polarizing impedance.

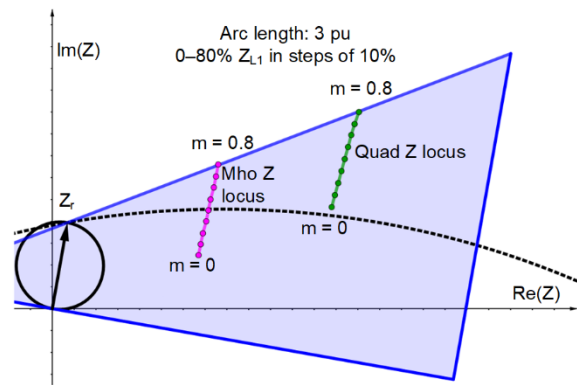


Fig. 12. Arc resistance impedance loci from 0 percent of the line to 80 percent (reach point) in 10 percent increments with negative 30-degree load angle during an AG fault. Dashed curve represents mho expansion.

In the same system, Fig. 13 simulates an AG fault at $m = 0.5$ pu with 1 pu (3.66 m, creepage distance across insulator) of arc length and tower footing of 3Ω . In Fig. 13a, the local and remote SIRs are both 50, and in Fig. 13b, the local SIR is 20 while the remote SIR is 4. The combination of arc resistance and tower footing impedance means that the apparent impedance is affected by both the local SIR and the infeed from the remote terminal. Even though Fig. 13a has a much higher local SIR than Fig. 13b, they both approach the dynamic mho boundary. This example highlights the need to look at the context of the system when assessing the apparent impedance.

Fig. 13a

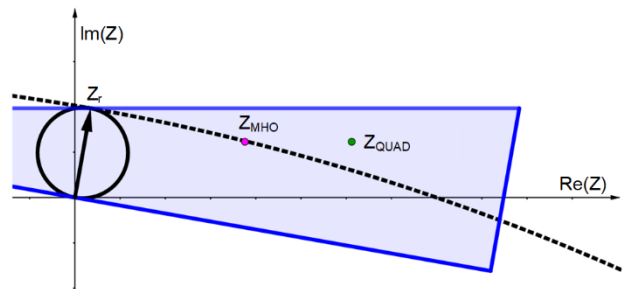


Fig. 13b

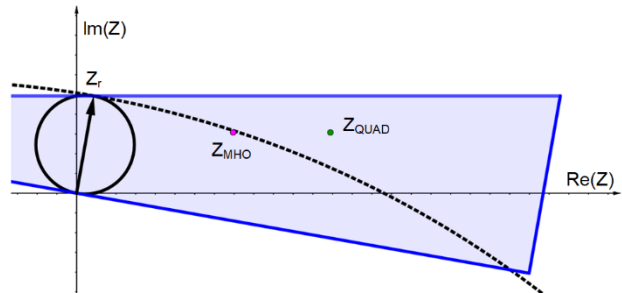


Fig. 13. Arc length of 1 pu with 3Ω tower footing impedance where $m = 0.5$ with no load flow, (a) SIR = 50 at local and remote sources, and (b) local SIR = 20 and remote SIR = 4.

Fig. 14 shows the apparent impedance for three-phase arcing faults at different SIRs for no load (Fig. 14a) and negative 30-degree load angle (Fig. 14b). The conductors are assumed to be arranged in an equilateral triangle for simplicity. The reactance blinder does not tilt during load flow because of the positive-sequence polarization. The resistive reach is reduced to 25 percent of the phase quadrilateral setting to prevent overreach during load export, as discussed in Section III.A.3. The lack of tilt also causes element underreach during load import conditions, as shown in Fig. 14b. A load export scenario causes the element to overreach, which is why the resistive reach is pulled back, as explained in Section III.A. This example highlights the need to include simulations with three-phase faults when examining the resistive coverage of impedance-based elements.

Fig. 14a

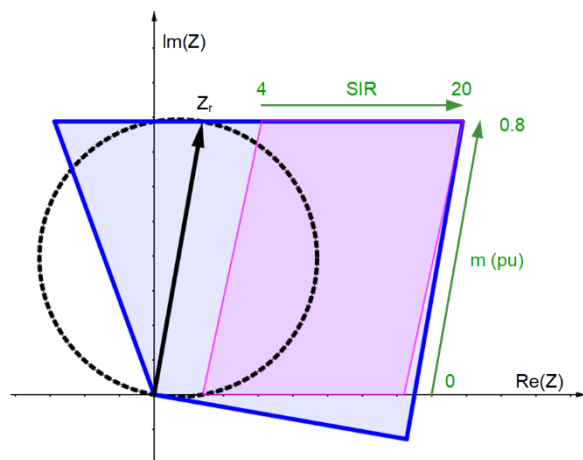


Fig. 14b

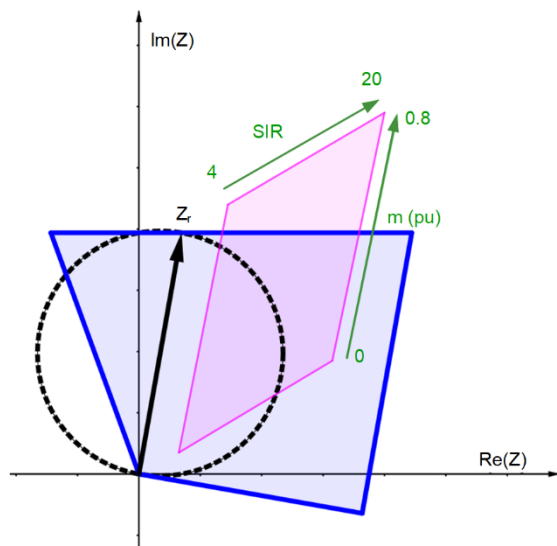


Fig. 14. Three-phase arcing impedance from an SIR of 4 to 20 at fault location 0 pu to the reach point 0.8 pu with 1 pu arc length, (a) no load flow and (b) negative 30-degree load angle.

Fig. 15 compares the apparent impedance of several AG arcing faults at different voltages with typical creepage distance data and instrument transformer ratios from Table V. There is no clear relationship between voltage level and apparent impedance during an arcing event. As the system voltage increases, so do the distance between conductors and the length of insulators. This increases the arcing voltage on the primary of the system, but the voltage measured at the relay is reduced by the higher ratio of the potential transformers at these higher voltages. The reach of 0.08Ω in Fig. 15 is too small to cover the arc resistance for the self-polarized mho, but it is within the resistive reach for the quadrilateral and the dynamic mho.

TABLE V
PARAMETERS FOR FIG. 15

System Voltage (kV)	PT Ratio (to 1)	CT Ratio (to 1)	Insulator Length (m)
500	4,500	400	3.66
240	2,000	400	1.75
138	1,200	240	1.31
69	600	80	0.61

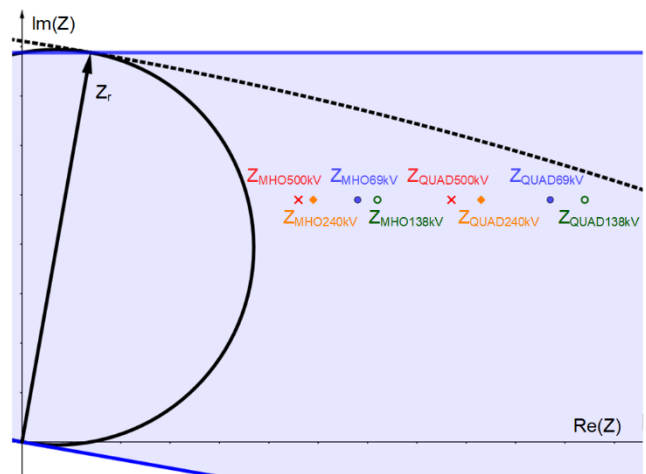


Fig. 15. Impedance plots of arc resistance at different voltages for an AG fault with typical insulator creepage.

From the above simulations in Fig. 11 to Fig. 15, if the impedance element cannot cover the arc resistance (plus tower footing for the ground fault), then it is not suitable for the application. Another important part of determining whether an element has appropriate resistive coverage is to perform fault studies using a target fault impedance, as described in the next subsection.

3) Target Impedance

Short circuit programs are used to determine the suitability of an impedance element for a desired sensitivity (maximum target fault impedance). This target can come from a utility's protection standard, which is based on years of service experience, or the requirements of an electric system operator. For example, the Alberta Electric System Operator (AESO) in Canada requires resistive coverage of 5Ω for ground faults on a bulk transmission line [45].

Fig. 16 shows the apparent impedance for a fault at 50 percent of a short line with an SIR of 13 at both ends. The relay reach is 0.4Ω with a target fault impedance of 5Ω primary. The mho element is right at the limit of the dynamic characteristic at a steady state; the quadrilateral element still has resistive coverage available.

Fig. 16a

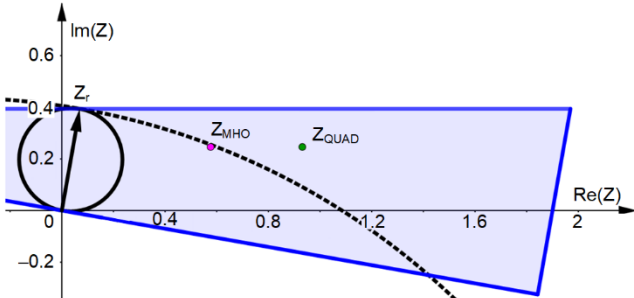


Fig. 16b

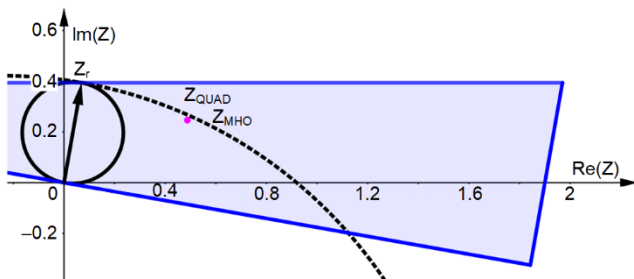


Fig. 16. Quadrilateral reach of 0.4Ω , no arc voltage, where $m = 0.5$, with 5Ω primary fault impedance, and $SIR = 13$ at both ends during (a) an AG fault and (b) BC fault.

In Fig. 17, the reach is increased to 1Ω and all other parameters remain the same. The increase in reach makes a significant difference in the resistive coverage. The dynamic mho circles (dashed) are shown at a steady state for BC and AG faults. This does not mean that a reach of 1Ω is always sufficient for this impedance target, as shown in the next example.

Fig. 17a

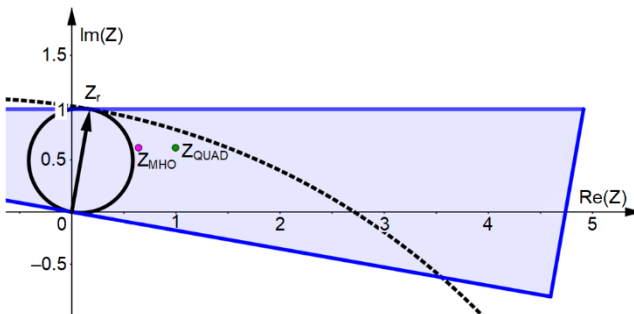


Fig. 17b

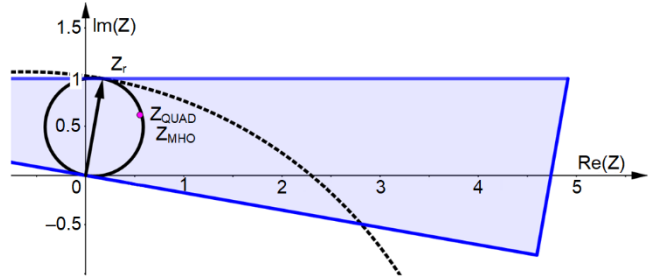


Fig. 17. Quadrilateral reach of 1Ω , no arc voltage, where $m = 0.5$, with 5Ω primary fault impedance, and $SIR = 13$ at both ends during (a) an AG fault and (b) a BC fault.

Fig. 18 maintains a 1Ω reach and fault parameters used in Fig. 17, but the remote SIR is reduced to four. With a smaller remote SIR, the infeed effect magnifies the apparent impedance calculated by the local relay. The apparent impedance for the mho touches the dynamic characteristic when the local SIR is 13 for an AG fault and 24 for a BC fault. These scenarios show that a reach setting of 1Ω secondary may not always be sufficient for the 5Ω primary target. It is not possible to have a rule-of-thumb setting for the minimum reach that applies to all scenarios, because the apparent impedance is too dependent on system conditions.

Fig. 18a

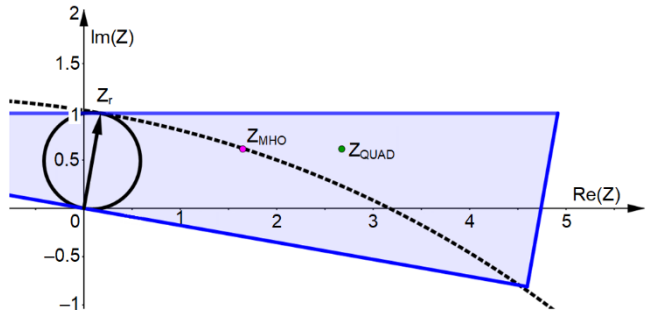


Fig. 18b

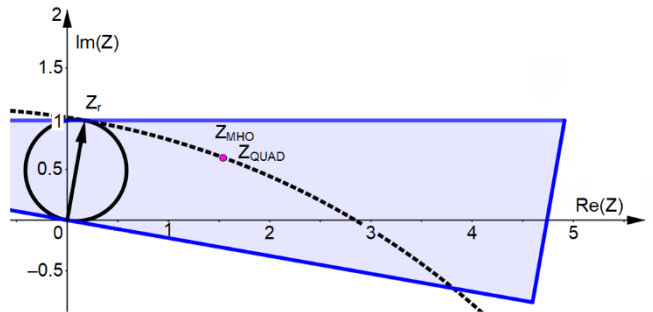


Fig. 18. Quadrilateral reach of 1Ω , no arc voltage, where $m = 0.5$, with 5Ω primary fault impedance, and remote $SIR = 4$, during (a) an AG fault with a local SIR of 13 and (b) a BC fault with a local SIR of 24.

E. Pilot Schemes

Communications-assisted schemes enhance dependability for faults with resistance on short lines and have a minor impact on security and speed. For short line protection, it is common to disable the instantaneous tripping zone and set the overreaching zone to 200 to 300 percent of the line or even up to 1,000 percent [3]. Load encroachment should be considered for those elements with a large reach. Otherwise, a permissive signal may become continuously keyed during load conditions. Fig. 19 shows an example of a permissive overreaching transfer trip scheme (POTT) that uses Zone 2 to send a permissive signal to the remote terminal and supervise incoming permissive signals.

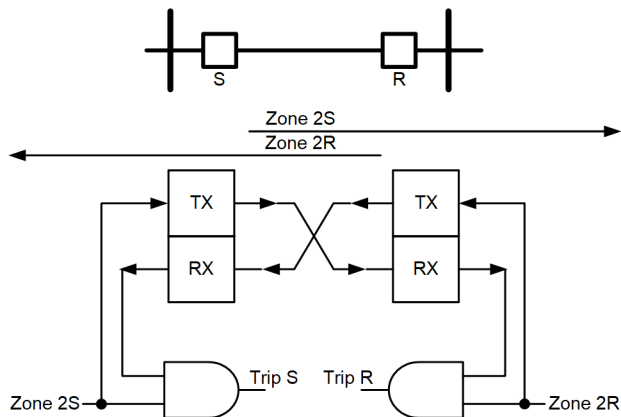


Fig. 19. POTT scheme with large overreach settings.

There are many options for transmitting a permissive or blocking signal, because the bandwidth for these schemes is very small, typically 0.5 to 1.5 kHz for analog channels and 9.6 kbps for digital channels [46]. Spread-spectrum solutions are one option that operates on an unlicensed band that provides good speed and noise immunity performance, and the range is ideal for lines that are geometrically short [47]. Optical fibers, microwaves, and power line carriers are also commonly used.

F. Mutual Coupling

Zero-sequence mutual coupling can be a significant challenge for ground distance and ground directional elements. When more than one line shares the same right-of-way through narrow corridors, zero-sequence current in one line can cause magnetic coupling to occur with the adjacent line and induce zero-sequence voltage. Zero-sequence voltage reversals due to mutual coupling on certain line configurations can jeopardize the security of elements polarized with zero-sequence voltage or current when faults are on an adjacent line [48]. Mutual coupling is not typically an issue for positive- and negative-sequence elements, because the summed flux from balanced currents is close to zero on the adjacent line.

Solutions to mutual coupling involve using negative-sequence for directional elements instead of zero-sequence, modifying k_0 , pulling back Zone 1 to prevent overreach, and ensuring Zone 2 does not underreach the remote bus [48]. Solutions that require reach pullback are generally not acceptable for short lines where the reach is already set small. It is not always realistic to apply an instantaneous Zone 1 mho

element on a line that has heavy mutual coupling because of the significant error and poor resistive coverage.

IV. DIRECTIONAL OVERCURRENT

Infeed reduces the resistive coverage and effectiveness of distance protection elements in looped systems, as described in Section III. The apparent impedance calculated by the local relay is magnified, because a portion of the voltage drop across the fault impedance is due to the (unmeasured) current from the remote bus. This is especially an issue for high-impedance ground faults that commonly occur due to vegetation and other debris. Directionally controlled ground overcurrent elements that use zero-sequence (67N) and negative-sequence (67Q) quantities are more sensitive, because the operating quantity does not use voltage. The limiting factors for overcurrent elements are the minimum pickup of the relay and the directional element requirements, both of which may require low levels of sequence voltage depending on the design. Table VI shows the sensitivity limitation for several different types of directional elements. Reference [49] discusses each type of directional element including the fundamentals.

TABLE VI
GROUND DIRECTIONAL OPERATING CHARACTERISTICS

Type	Operating Principle	Polarizing Quantity	Sensitivity Limitation
1	Torque	V_2 or V_0	One or more of the following: a) Minimum sequence voltage (V_2 or V_0) b) Minimum sequence current (I_2 or I_0) c) Minimum net torque (sequence voltage times current)
2	Torque	I_0	Minimum I_0 threshold
3	Sequence impedance thresholds (Z_2 or Z_0)	V_2 or V_0	Minimum sequence current (I_2 or I_0), and minimum unbalance ratio $\frac{ I_2 }{ I_1 }$ or $\frac{ I_0 }{ I_1 }$

Example calculations are performed in [43] to determine the resistive coverage for nine relays that use different directional operating principles and to determine minimum thresholds for maximum sensitivity. The results of the comparison show that elements using sequence impedance thresholds have high levels of sensitivity [43]. Using the idea of resistive coverage plots in [43], References [46], [50], and [51] compare the sensitivity for several elements on different lines including ground overcurrent elements (67Q and 67N), distance elements (21MG and 21XG) and line current differential elements using negative sequence and zero sequence (87LQ, 87LG). Fig. 20 shows a sensitivity chart without vertical axis labels to keep the conclusions general. Communications-assisted tripping schemes can also be used for overcurrent elements to achieve high-speed tripping while avoiding overreaching issues since their reach is not well-defined in looped systems.

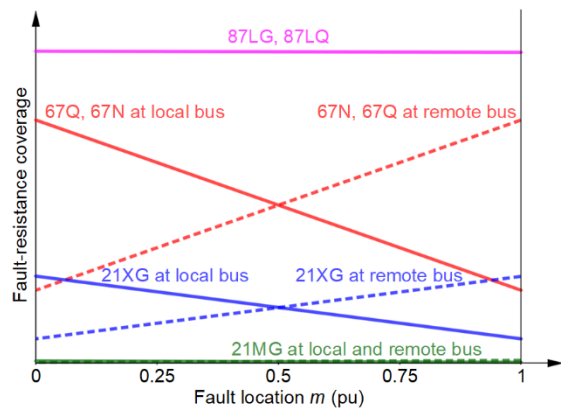


Fig. 20. Fault-resistance coverage for different phasor-based algorithms on a short line with a double circuit tower and parallel line.

As shown in Fig. 20, 67N and 67Q are often two to three times more sensitive than quadrilateral elements (21XG) and an order of magnitude more sensitive than ground mho elements (21MG). 67Q has an advantage over 67N, because it can be applied to lines that have strong zero-sequence mutual coupling. There may be slight differences in resistive coverage between 67Q and 67N for close-in or remote faults depending on the differences in the negative- and zero-sequence networks. 87L has the best resistive coverage and is discussed in the next section.

Directionally controlled overcurrent elements that are high-set or used in a pilot scheme have their own unique issues, which do not affect impedance-based methods. The reach for overcurrent elements changes with the system impedance, but the reach for distance elements is well defined. Ground overcurrent elements are also susceptible to system unbalances due to nontransposed lines, inline switching (momentary breaker pole discordance), and open-phase conditions. One possible solution is to use time-delayed elements that account for switch operate time plus a safety margin, but this does not solve unbalances that are systemic (untransposed lines) or may exist for longer periods of time (open-phase), unless the relay also has special logic to detect these events [50].

Most phasor-based relays calculate current magnitude using a digital filter data window [52]. The speed of the overcurrent element is proportional to the ratio of the applied signal divided by the pickup setting [53]. When the measured current is much higher than the pickup setting, the element can operate at subcycle speed. Fig. 21 shows maximum and minimum speed curves from one phasor-based protective relay. Directionally controlled overcurrent elements add extra processing time compared to nondirectional elements.

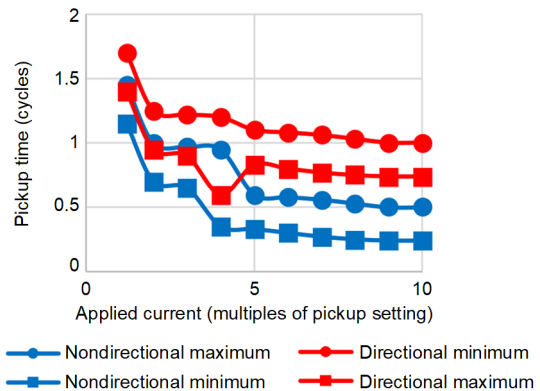


Fig. 21. Overcurrent pickup time versus applied current [34].

V. LINE CURRENT DIFFERENTIAL

Line current differential solutions are based on Kirchhoff's current law, which states that the sum of currents entering a node must equal zero. In a practical installation, relays at each terminal exchange measured current information over a communications channel, align the data, and determine whether a fault exists in the zone. The algorithm must be sensitive enough to detect high-impedance faults, but also maintain security for several errors, such as capacitive line charging current, CT saturation, channel asymmetry and delay, and unmonitored tapped lines.

Two methods of implementing line current differential in phasor-based relays are using a percent differential characteristic or using the alpha plane [54]. The percentage restrained differential method, shown in Fig. 22, calculates an operate quantity I_{OP} and a restraint quantity I_{RT} for the N terminals, as shown in (18) and (19).

$$I_{OP} = |I_1 + I_2 + \dots + I_N| \quad (18)$$

$$I_{RT} = p(|I_1| + |I_2| + \dots + |I_N|) \quad (19)$$

where:

p is a constant.

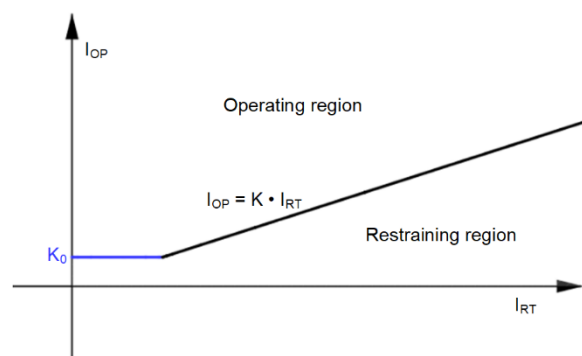


Fig. 22. Percentage restrained differential characteristic (single slope is shown).

The operate condition is defined in (20).

$$I_{OP} = K \cdot I_{RT} \text{ and } I_{OP} > K_0 \quad (20)$$

where:

K is a constant representing the slope of the characteristic.

K_0 is the minimum operate current sensitivity.

Relays typically have one to two slopes, which may be fixed or dynamically switch between a high-security slope and low-security slope based on external fault detection logic [55].

The alpha-plane method calculates the complex ratio of the remote current I_R divided by the local current I_L , as shown in (21).

$$r = \frac{I_R}{I_L} \quad (21)$$

The ratio r is plotted on the complex plane and compared with a characteristic (Fig. 23) that is shaped to provide security for CT saturation, asymmetry, infeed, outfeed, and other errors [54].

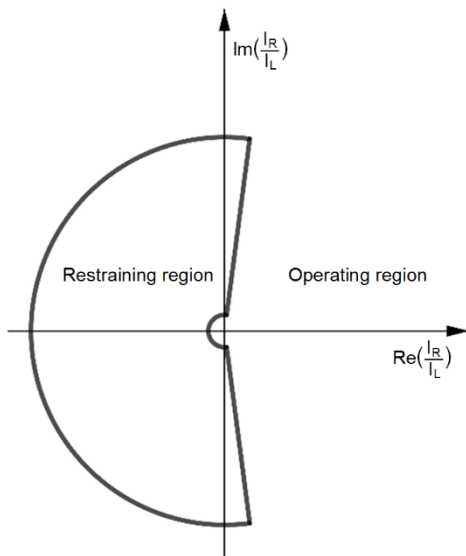


Fig. 23. Alpha-plane differential characteristic.

An enhancement to this algorithm is called the generalized alpha plane [56] that allows for any number of terminals, transformers in the zone of protection, current charging compensation, and a high-security mode with an expanded characteristic when external faults are detected.

Line current differential is one of the best solutions for short line protection with few downsides. The following lists show the pros and cons for 87L protection.

Pros:

- Can protect extremely short lines, which have relatively low charging current and generally do not require algorithms that use voltage for compensation [56]. Therefore, there is no concern about loss of potential or CVT transients for 87L.
- Has no need to coordinate with external protection.
- Is almost immune to effects of infeed, power swings, mutual coupling, cross country faults, intercircuit faults, SIR, and line loading.

- Uses current only (does not require directional elements).
- Can detect faults on a per-phase basis (87A, 87B, 87C) and also detects faults using negative-sequence (87Q) and zero-sequence (87G) quantities.* The latter two options have better sensitivity than impedance or directional overcurrent elements, as shown in Fig. 20 [46].
- Has the potential for subcycle operation depending on the applied differential current and relay algorithm.†
- Accommodates reasonable levels of outfeed depending on the characteristic.

Cons:

- Requires a dependable and deterministic communication channel, which is typically 64 kbps bandwidth [56].
- May require GPS or terrestrial time signal for channels with high levels of asymmetry.†
- Must consider a backup/failover method if there is a channel failure.
- Is usually slower than time-domain technologies.
- Has a limited number of terminals that can be used in the scheme based on the relay design.

* Modern line current differential solutions.

† Relay/manufacture dependent.

One area where 87L requires investigation is when series capacitors are used. Subharmonic-frequency oscillations may be a concern in the presence of series capacitors. This should be investigated with transient studies [57].

For the special case where series capacitors are installed inside the zone of protection, a current inversion can occur, as shown in Fig. 24 [57]. If the fault current is high enough, the series capacitor is bypassed across a triggered air gap or spark gap [58]. If the fault current is low, such as for a high-impedance fault, the capacitor may remain in the fault path. When X_C remains connected to the system during a fault, a current inversion occurs if X_C is greater than the remote impedance Z_R . This may cause the relay to restrain depending on the magnitude of the local and remote currents during the fault. Fortunately, internal series capacitors are unlikely to be an issue for short lines, because the line impedance is generally too small to justify their installation.

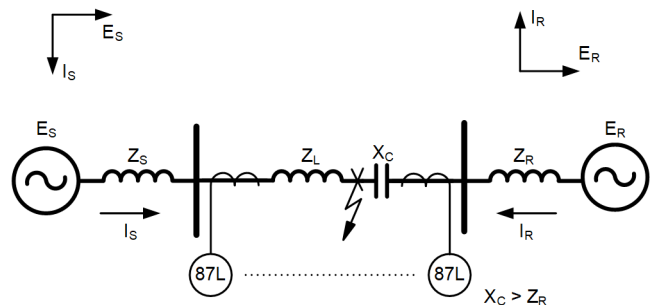


Fig. 24. Fault on transmission line with internal capacitor.

VI. INCREMENTAL DISTANCE ELEMENT (TD21)

Incremental quantities (i.e., superimposed quantities) are the change in voltage and current from pre-fault to post-fault states over a short time interval, usually a power system cycle [59]. This provides short-lived quantities that are not affected by load flow, can be made fast and secure, and are suited for protection with nontraditional sources, because the driving source in the incremental network is the fault point.

One implementation of a TD21 incremental distance element provides a distance-like function using incremental quantities [2]. Consider the line in Fig. 25 with the resistance R , the inductance L , and the relay measured voltage $v(t)$ and current $i(t)$.

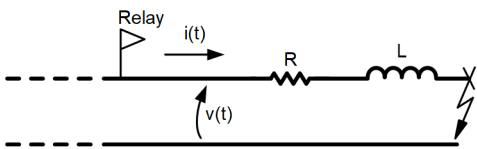


Fig. 25. Time-domain relay facing a forward fault on the line.

The voltage at the relay in the time domain is calculated as shown in (22).

$$v(t) = R \cdot i(t) + L \frac{di(t)}{dt} \quad (22)$$

Equation (22) is manipulated to introduce a new variable i_Z , the replica current in (23) and (24). For convenience, function notation is dropped, but it is implied that voltage and current are still functions of time.

$$v = |Z| \cdot i_Z \quad (23)$$

where:

$$i_Z = \frac{R}{|Z|} \cdot i + \frac{L}{|Z|} \frac{di}{dt} \quad (24)$$

The replica current i_Z is the voltage drop across a scaled replica of the line impedance Z with a magnitude of 1Ω . Replica current is convenient, because it simplifies differential equations to more familiar algebraic equations, and solving homogeneous resistor-inductor (RL) circuits is as easy as solving dc circuits. Replica currents do not have any appreciable decaying dc components.

Fig. 26 shows a fault on a line at m per unit with replica current i_Z and voltage at the fault point v_F .

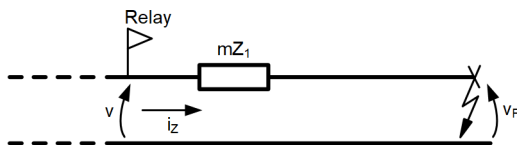


Fig. 26. Time-domain relay measuring replica current for a fault on the line.

Equation (25) can be used to solve for v_F .

$$v_F = v - m \cdot |Z_1| \cdot i_Z \quad (25)$$

Express the fault voltage in (25) as an incremental quantity in (26), and replace the per-unit distance to the fault m with the relay reach setting TD21M:

$$\Delta v_F = \Delta v - \text{TD21M} \cdot |Z_1| \cdot \Delta i_Z \quad (26)$$

During a fault, the relay uses (26) to determine Δv_F under the assumption that the fault occurs at the reach point. If a bolted fault occurs at the reach point, as shown in Fig. 27, then $|\Delta v_F|$ is equal to the pre-fault voltage V_{PRE} .

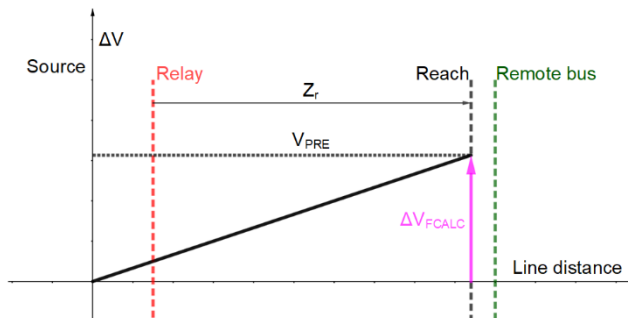


Fig. 27. $\Delta v_F = V_{PRE}$ for a bolted fault at the reach point.

Fig. 28 shows an internal fault F1 and an external fault F2. F1 is inside the reach, and the relay measures a larger Δi_Z than a fault does at the reach point. Therefore, (26) calculates $|\Delta v_F|$ greater than V_{PRE} ($\Delta v_{FCALC|INT}$). F2 is outside the reach. Therefore, the relay measures a smaller change in Δi_Z , so (26) calculates $|\Delta v_F|$ less than V_{PRE} ($\Delta v_{FCALC|EXT}$).

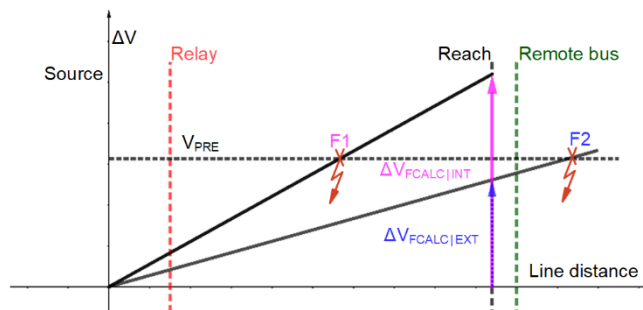


Fig. 28. $|\Delta v_F|$ is greater than $|V_{PRE}|$ for an internal fault. $|\Delta v_F|$ is less than $|V_{PRE}|$ for an external fault.

The condition to operate is shown in (27).

$$|\Delta v_F| > |V_{PRE}| \quad (27)$$

TD21 is also supervised by the incremental quantity directional element TD32 and the overcurrent element OC21 [2]. TD32 is discussed in Section VII. The OC21 element maintains security and prevents overreach by ensuring there is an appreciable voltage difference between faults at the remote bus and faults at the reach point. This is similar to the requirement of one utility described in Section III when it evaluates the security and suitability of an underreaching distance element on a short line. Equation (28) shows the change in voltage at the relay for a fault at the reach point Δv_{reach} , and (29) shows the change in voltage at the relay for a fault at the remote bus Δv_{remote} .

$$\Delta v_{reach} = \Delta v - \text{TD21M} \cdot |Z_1| \cdot \Delta i_Z \quad (28)$$

$$\Delta v_{remote} = \Delta v - |Z_1| \cdot \Delta i_Z \quad (29)$$

The difference between (28) and (29) defines the minimum-security voltage V_{MIN} , as shown in (30).

$$V_{\text{MIN}} < (1 - \text{TD21M}) |Z_1| \cdot |\Delta i_Z| \quad (30)$$

For faults on short lines, most of the voltage drop is across the source impedance and the slope of the Δv profile across the line is small. Therefore, the fault current must be larger for short lines than for long lines to have enough of a voltage change to pass the security requirement.

Assuming V_{MIN} is 5 percent of nominal voltage V_{NOM} , (31) is solved for the minimum change in replica current required for TD21 to operate.

$$|\Delta i_Z| > \frac{0.05 \cdot V_{\text{NOM}}}{(1 - \text{TD21M}) |Z_1|} \quad (31)$$

Equation (31) is the overcurrent element equation for OC21, which is evaluated by integrating the calculated replica current on a sample-by-sample basis [2].

The OC21 pickup threshold, which is found using (31), shows that the current requirement is higher for shorter lines (smaller $|Z_1|$) and lines with a larger reach setting (TD21M). This maintains security for short lines, but at the expense of dependability, because the high SIR reduces the fault current available.

To test the dependability, a relay was programmed with positive-sequence line impedance $Z_{\text{1MAG}} = 4$ and reach $\text{TD21M} = 0.7$. Faults were applied at 10 percent increments of the reach for SIR values of 1, 2, 3, and 4. Each point in Fig. 29 represents the percentage of operations that occurred out of 50 faults that were initiated at random points on the wave.

As the SIR increases to three and above, the dependability of the TD21 decreases and it is less suitable for electrically short lines. Reference [60] shows that the operating time also increases with the SIR for TD21.

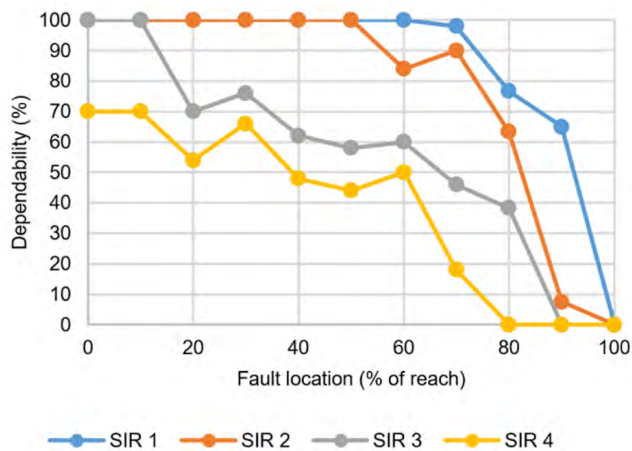


Fig. 29. SIR effects on TD21 dependability.

VII. INCREMENTAL DIRECTIONAL ELEMENT (TD32)

Reference [61] explains the detailed theory of incremental quantity directional element TD32, and [60] shows the implementation. To summarize the basic theory, forward faults produce a change in voltage, as shown in (32).

$$\Delta v = -|Z_S| \cdot \Delta i_Z \quad (32)$$

where:

Z_S is the source impedance behind the relay.

Δv has the opposite polarity of Δi_Z .

The difference in polarity is explained by considering Δv and Δi_Z in the time domain. If the fault occurs during the positive half of the voltage sine wave, the voltage drops to zero (negative Δv) and the replica current becomes more positive (positive Δi_Z). If the fault occurs during the negative half of the voltage sine wave, the voltage *increases* to zero (positive Δv) and the replica current becomes more negative as its magnitude grows (negative Δi_Z).

Faults in the reverse direction produce a change in voltage, as shown in (33).

$$\Delta v = |Z_L + Z_R| \cdot \Delta i_Z \quad (33)$$

where:

Z_L is the line impedance.

Z_R is the remote source impedance.

In this case, Δv and Δi_Z have the same polarity, because the current for a reverse fault enters the nonpolarity side of the CT (assuming the standard practice of installing CTs to measure current into the line as positive).

To determine operation, an operate quantity S_{OP} is created, as shown in (34).

$$S_{\text{OP}} = -\Delta v \cdot \Delta i_Z \quad (34)$$

The negative sign in (34) ensures S_{OP} is positive for forward faults and negative for reverse faults. The forward and reverse thresholds (S_{FWD} and S_{REV}) in (35) and (36) are created by substituting (32) and (33) into (34), shown as follows. Z_{FWD} is a fraction of Z_S , and Z_{REV} is a fraction of Z_L . Δ_{MIN} is a small security margin.

$$S_{\text{FWD}} = Z_{\text{FWD}} (\Delta i_Z)^2 + \Delta_{\text{MIN}} \quad (35)$$

$$S_{\text{REV}} = -Z_{\text{REV}} (\Delta i_Z)^2 - \Delta_{\text{MIN}} \quad (36)$$

The relay declares forward if $S_{\text{OP}} > S_{\text{FWD}}$. The relay declares reverse if $S_{\text{OP}} < S_{\text{REV}}$.

The TD32 element is ideal for a POTT scheme, because the impedance threshold characteristics ensure great sensitivity. Security is achieved with built-in time-domain overcurrent element OC32 that is integrated like the OC21 element, except with a threshold that is 10 percent of the relay channel rating (5 A or 1 A). TD32 is not limited by the OC21 equation that prevents the TD21 element from overreaching. The POTT scheme also has a user-settable overcurrent threshold to ensure that the event has enough energy to be considered a fault and to prevent misoperations when switching inline capacitors [2].

The combination of sensitivity, security, and typical operate times of 2 ms and under [60] makes TD32 ideal for short lines in a permissive scheme. A simulation of TD32 performance is included in the next section.

VIII. TW87

A. TW87 Basic Theory

Advancements in analog-to-digital (A/D) converters have made true TW relays based on MHz samples a reality [61]. TWs are used in a variety of applications including fault location [62], continuous disturbance monitoring to detect faults before they occur [63], and protective relaying algorithms to achieve 1 to 2 ms tripping times depending on line length [2]. Reference [61] explains the theory of the TW differential element TW87, and [60] shows the implementation. A summary is provided in this section.

When a fault occurs on a transmission line, it launches voltage and current TWs in both directions, as shown in Fig. 30. The magnitudes and arrival times of incoming TWs are recorded at each terminal using high accuracy time stamps and exchanged between relays across a high-speed channel.

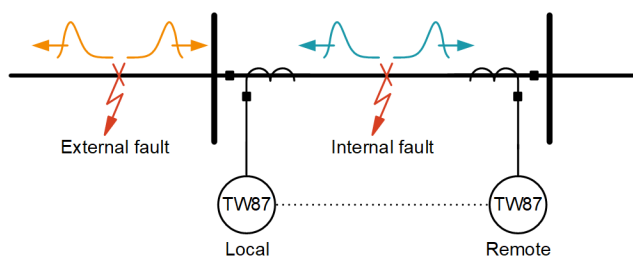


Fig. 30. TW propagation for internal and external faults on a transmission line.

The first TWs to arrive at each terminal, i_{TWL} and i_{TWR} , are time-aligned using the time-shifted difference in the TW arrival times, ΔT . The operate current I_{OP} is calculated in (37).

$$I_{OP(t)} = i_{TWL(t \pm \Delta T)} + i_{TWR(t)} \quad (37)$$

For internal faults, the first wave seen by the relay at each terminal has the same polarity and I_{OP} is large. For external faults, the first waves measured by the relays at each terminal have opposite polarity (because of the CT polarity) and I_{OP} is small.

To maintain security, a restraining signal is calculated by recognizing that for external faults, the wave first arrives at one terminal, and then after the TW line propagation time (TWLPT), it exits the other end of the line. The polarity of the waves is opposite of each other, because the CT polarity marks are facing away from the line at each end. Each terminal calculates its local restraining current I_{RTL} , as shown in (38).

$$I_{RTL(t)} = |i_{TWL(t - TWLPT)} - i_{TWR(t)}| \quad (38)$$

The restraint currents are exchanged between each relay, and the overall restraint I_{RT} is the maximum of the two. From (38), the restraint current is large for external faults, because entering and exiting waves are measured as opposite polarity and occur time TWLPT apart. The element operates if $I_{OP} > k \cdot I_{RT}$, where k is an internal relay setting for the restraining factor.

TWs are extracted using a differentiator-smoother filter, as shown in Fig. 31 [62].

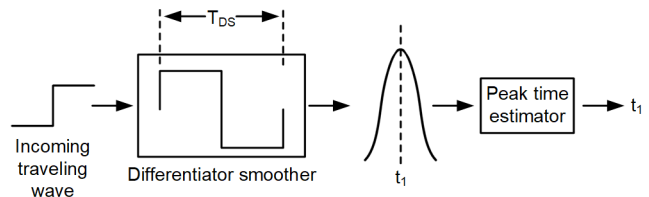


Fig. 31. TW peak time extraction using the differentiator-smoother filter.

The combination of smoothing and differentiating the input signal reduces distortions in the incoming TW and allows for interpolation to accurately estimate the time of the peak [62]. One relay uses a window length T_{DS} of 20 μs that provides a time-stamp resolution of 0.2 μs [2]. This is important for short lines or any internal fault that is close to a bus with a TW relay where the reflections can overlap within the data window, as shown in Fig. 32. This paper refers to sections of the line where a fault causes more than one TW in the filter window as filter reflection zones. These zones exist near bus terminals and tapped sections of the line.

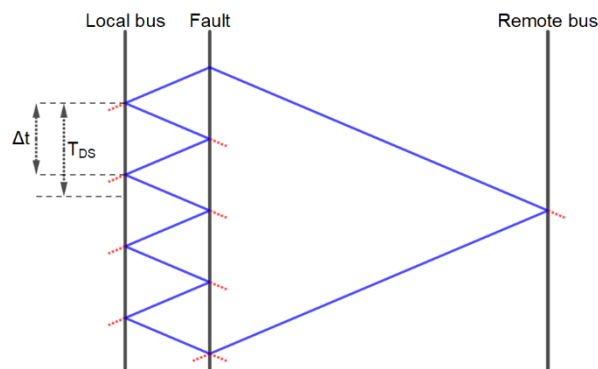


Fig. 32. TW reflections shown on a Bewley diagram for a fault close to the local bus.

If Δt in Fig. 32 is less than T_{DS} , reflections will cause more than one wave to appear within the filter window and potentially interfere with the relay's ability to either recognize the peak of the first wave or calculate the proper time stamp. The result is that the relay may throw away the bad wave data and restrain, or it may operate and additional error is present in the fault location algorithm. For long lines, this is not a concern, because the filter reflection zones near terminals are a small percentage of the total line length, and backup protection elements are suited to clear close-in faults quickly (21, TD21, 67, POTT, etc.). But if the line is short enough, the entire line can be a filter reflection zone.

For a fault on a line with length LL , $\Delta t \geq T_{DS}$ must be true to prevent reflection overlap within the data window:

If the fault occurs at 50 percent of the line, then $\Delta t = TWLPT$. For the worst-case scenario when $TWLPT$ and T_{DS} are equal, the minimum line length LL_{min} is calculated in (39) to ensure that a fault at the midpoint of the line has no reflections in the filter window, along with the first arriving wave.

$$LL_{min} = k_{vel} \cdot c \cdot T_{DS} \quad (39)$$

where:

c is the speed of light in m/s.

k_{vel} is the propagation speed of the wave in pu of c .

T_{DS} is the filter window in seconds.

LL_{min} is proportional to k_{vel} , so lines with slower propagating waves (such as cables) can be shorter without overlap in the filter.

Consider an example with a line that has $k_{vel} = 0.97$ and $T_{DS} = 20 \cdot 10^{-6}$ s, then LL_{min} is approximately 5.8 km. A fault at 50 percent of the line ensures that no reflections between the fault point and relays are inside the differentiator-smoother data window at the same time as the first arriving wave. If the fault is placed closer to either terminal, it resides within a filter reflection zone and the data window is shared with a reflection from the fault point.

B. EMTP Model

To investigate the performance of TW87 in the presence of reflections, an EMTP model was created for a 6 km line, as shown in Fig. 33.

Parallel impedances are included at each source end with switches that are open or closed depending on the simulation. The characteristic impedance of the line is the same as each individual parallel impedance. The current reflection coefficient Γ_i is controlled for each simulation depending on the number of connected parallel lines, as shown in (40) [64].

$$\Gamma_i = \frac{Z_{c1} - Z_{cP}}{Z_{c1} + Z_{cP}} \quad (40)$$

where:

Z_{c1} is the characteristic impedance of the line.

Z_{cP} is the characteristic impedance of the parallel combination of the source lines.

If only one source line is connected, then $Z_{cP} = Z_{c1}$ and $\Gamma_i = 0$ (no reflections). If two parallel lines are connected, $Z_{cP} = 0.5 \cdot Z_p$, and $\Gamma_i = 0.33$. For ten parallel lines, $\Gamma_i = 0.82$.

The simulation was conducted at 2 MHz using the JMARTI line model that simulates frequency-dependent effects of transmission lines, which are important for accurate TW simulations [65]. The output files from the simulation were converted using relay-specific software and uploaded to the relays for built-in playback [66]. The conversion process also applies the relay's analog filters for accuracy [2].

A line energization test was conducted to determine the TWLPT for this short line. The local breaker was closed while the remote breaker was open, and the resulting TWs are shown in Fig. 34. Since the local breaker closed at a zero-crossing for Phase A, only the current waves for Phases B and C are visible. The time difference between waves represents twice the TWLPT since the waves travel to the remote end of the line and then are reflected to the local terminal.

Simulations were performed for several different reflection coefficients (Γ_i) by closing the switches at each source end and paralleling a different number of source lines including two, four, six, eight, and ten. This corresponds to reflection coefficients of 0.33, 0.6, 0.71, 0.78, and 0.82, respectively. AG faults were applied from 0 to 50 percent of the line in 10 percent increments for each combination of connected parallel source lines. The performances of TW87, TD32, and TD21 are examined for all scenarios.

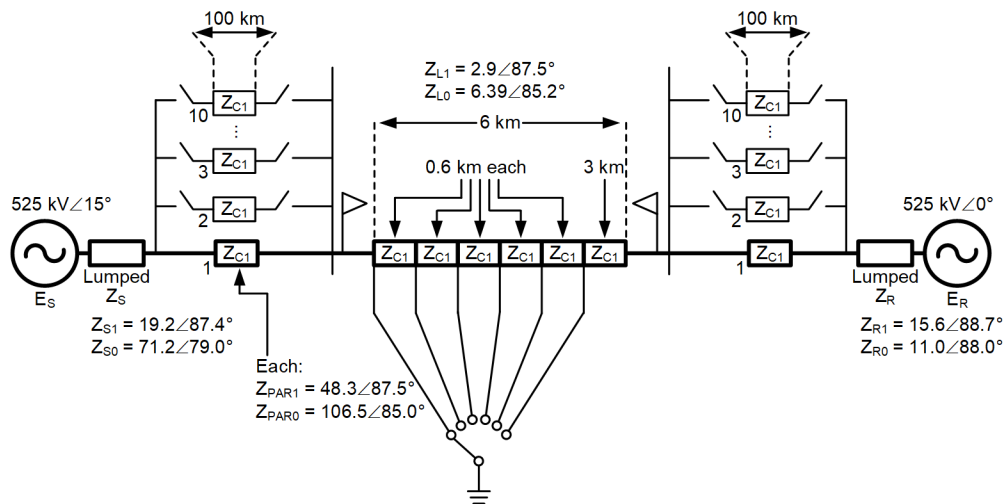


Fig. 33. EMTP model is shown for short line simulations. Relays are represented as flags looking into the 6 km line.

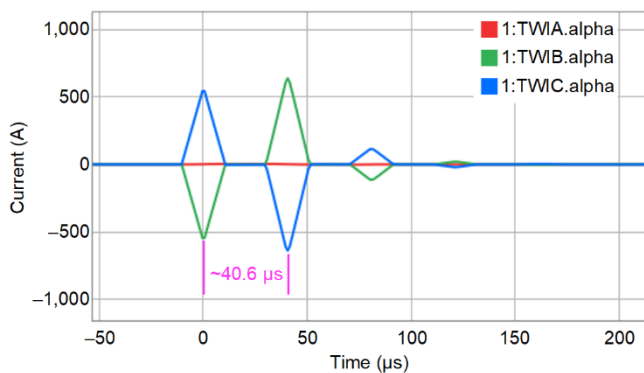


Fig. 34. Line energization test is conducted. TWLPT is half the time between peaks.

C. Simulation Results

Fig. 35 shows the voltages, currents, and select binary digitals from a COMTRADE file of an AG fault at 10 percent of the line with six parallel source line impedances connected ($\Gamma_i = 0.71$). The TW87 element operated in 775 μs , TD32 operated in 1,475 μs , and TD21 did not operate.

TD21 did not operate for faults in any scenario, because the lowest SIR is approximately 8.3 when all parallel source lines are connected (Fig. 33). The OC21 threshold is too high for this short line, as explained in Section VI.

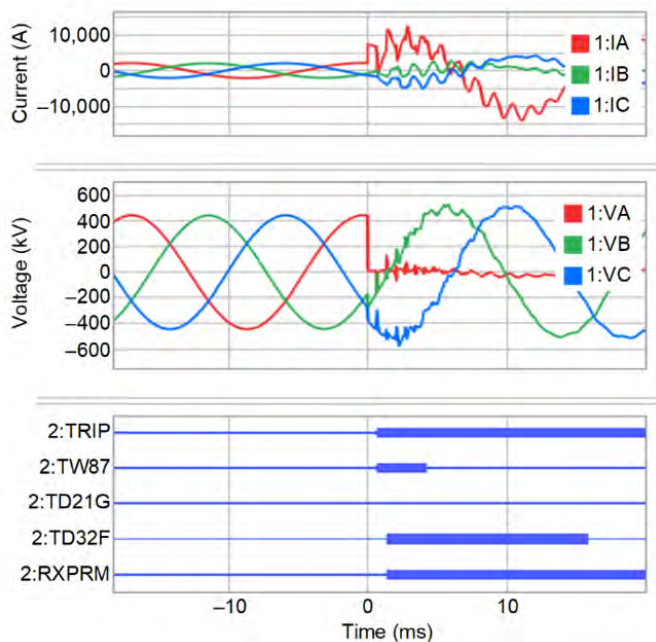


Fig. 35. High-resolution event report for AG fault at 10 percent of the line.

The POTT scheme based on TD32 operated for all faults in all scenarios, making it a great performer for short line protection.

TW87 performance depended on the location of the fault and the coefficient of reflection (Γ_i). Table VII is a summary of TW87 operation based on fault location and Γ_i . The number of parallel source lines used in each simulation is listed next to each reflection coefficient.

TABLE VII
TW87 OPERATION (Y/N)

Parallel Lines	Γ_i	Fault Location					
		0%	10%	20%	30%	40%	50%
2	0.33	Y	Y	Y	Y	Y	Y
4	0.60	Y	Y	Y	N	Y	Y
6	0.71	Y	Y	N	N	Y	Y
8	0.78	Y	Y	N	N	Y	Y
10	0.82	Y	N	N	N	Y	Y

When Γ_i is small, TW87 operates for all internal fault locations, even when the fault is close enough to the bus to see many reflections within the filter window. As Γ_i becomes greater, TW87 does not operate for a larger portion of faults in the area where reflections will occur within the filter window. One exception is when the fault is very close to the local bus or directly on the bus.

Fig. 36 shows the waveforms for Phase A during AG faults at 10 percent of the line (blue), 30 percent of the line (green), and 50 percent of the line (red). All ten parallel source lines are connected ($\Gamma = 0.82$). The top graph shows IA for each fault in the time domain; the jagged staircase property of each waveform indicates the number and magnitude of the reflections.

The bottom graph in Fig. 36 shows the extracted TW output from the differentiator smoother. For a fault at 50 percent of the line (red), the initial wave and subsequent reflection waves are about 20 μs apart, as expected. The differentiator smoother extracts each wave without any overlap in the filter, and the output has a clear peak for each wave. When the fault is applied at 30 percent (green), reflections appear in the filter window along with the initial wave. The TW output looks like a decaying function that can confuse the relay's ability to recognize the initial wave. For a fault very close to the local bus at 10 percent (blue), there are so many reflections that the output from the filter looks like one large wave with decay. This wave has a larger amplitude and faster decay than the wave at 30 percent. The relay may process this wave and allow TW87 to operate.

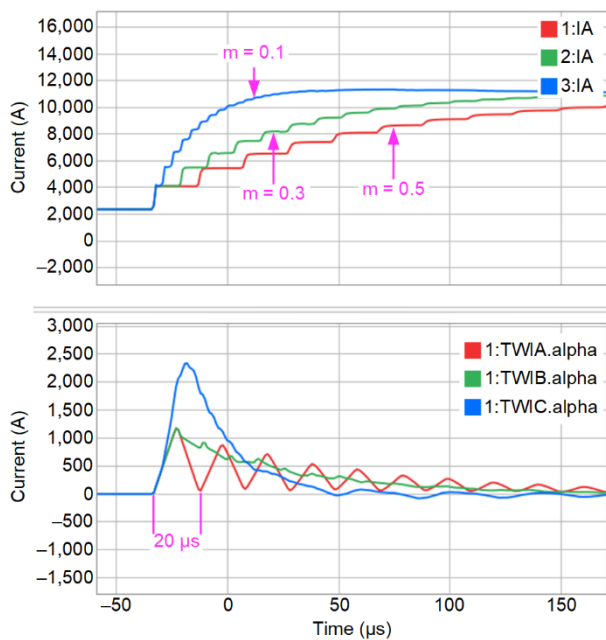


Fig. 36. AG fault at different points on the line: 50 percent (red), 30 percent (green), and 10 percent (blue). Reflections in the time domain (top graph). Extracted TWs from the differentiator smoother (bottom graph).

The TW fault location error calculated using the double-ended method is greater in the areas where significant reflections occur within the filter window and with higher reflection coefficients, as shown in Fig. 37.

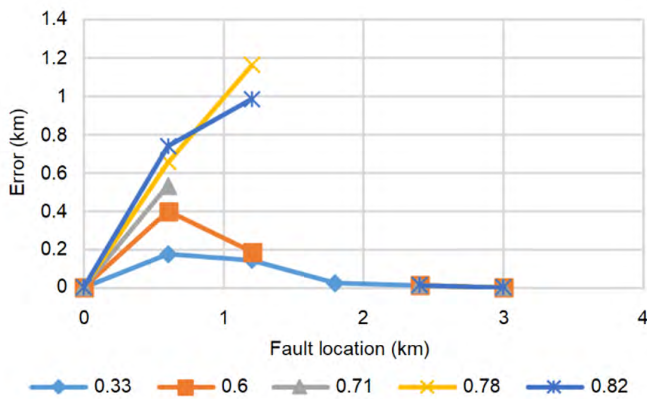


Fig. 37. Fault location errors show when the fault is close to the local bus. Points that are not plotted indicate the relay did not return a location for the double-ended TW fault locator.

The results of the simulation show that TW87 can be used to help accelerate tripping on geometrically short lines for faults at certain locations, but dependability is reduced for faults within reflection zones when the reflection coefficient is high. Longer lines also have reflections for faults that occur near a terminal, but these faults are a small percentage of the total faults because of the line length, and they are covered by other traditional elements that operate quickly for close-in faults.

IX. CONCLUSION

Table VIII summarizes the general performance of the different elements examined in this paper.

TABLE VIII
SHORT LINE PROTECTION PERFORMANCE BY ELEMENT

Element	Rating	Notes
87L	Best	Dependable and extremely sensitive. Higher bandwidth than pilot schemes. Slower than time-domain methods. Immune to power swings and mutual coupling. Tolerant of series-compensated lines. Voltage not required for capacitive compensation on short lines.
TD32 (POTT)	Great	Dependable, sensitive, and with a low bandwidth. Relatively immune to power swings and series compensation issues. Extremely fast operation: 2 ms and below for short lines. Excellent for nontraditional sources.
21M/21X (Pilot)	Good	Low bandwidth; susceptible to power swings, series compensation, and mutual coupling issues.
67N/Q (Pilot)	Good	More sensitive than 21M/21X pilot for unbalanced faults. Low bandwidth. Variable reach based on the system configuration.
21X	Satisfactory	Better resistive coverage than 21. Resistive reach limited by measurement errors.
TW87	Requires study	Fastest protection method with great security. 1 ms and below for short lines. Tripping for faults in certain locations can be accelerated on a short line. Dependability for faults within reflection regions depends on the reflection coefficient.
21M	Not recommended	Poor resistive coverage for the focus of this paper—underreaching instantaneous elements. Overreaching step-distance backup is acceptable.
TD21	Not recommended	Reduced dependability when SIR is more than 2.5.

where:

21M = mho distance

21X = quadrilateral distance

67N = directional zero-sequence overcurrent

67Q = directional negative-sequence overcurrent

87L = phasor line current differential (phase, negative sequence, ground)

TD21 = time-domain distance-like element

TD32 = time-domain directional

TW87 = TW differential

The best solutions require communications between the relays involved in the scheme. Phasor-based 87L is one of the best solutions if a reliable channel and bandwidth are available because of its high sensitivity, immunity to most system conditions that can affect 21 and 67 elements, and reasonable speed. Without communications, the best solution is often quadrilateral (21X) with its resistive reach advantage over the mho element (21) and well-defined reach over directional overcurrent elements (67). One option to explore for a traditional backup is time-delayed 67N to distance elements without communications.

For time-domain technologies, TD32 used in a POTT scheme is a very strong performer with great sensitivity and security. TD32 is consistently much faster than phasor-based solutions with a minimal bandwidth requirement. It is also one of the best suited for nontraditional sources since the incremental quantities used by the algorithm are driven from the fault point instead of the source. TD32 is also relatively unaffected by issues arising from power swings and series-compensated lines that can affect 21 and 67 solutions. However, the TD21 element is not suitable for short lines, because the dependability is reduced when the SIR is greater than 2.5.

TW87 is the fastest algorithm that can accelerate tripping for faults in certain locations on a geometrically short line without sacrificing security. Dependability is affected by the reflection coefficient for faults within areas where multiple reflections occur within the filter window. There is no harm in enabling the element for short line protection, but it requires other elements to provide backup. Reflection issues near terminals are not a concern for medium and long lines, because the affected portion of the line is very small compared to the overall line length. Faults near terminals are also cleared by traditional backup elements that operate very quickly for close-in faults with no intentional time delay.

X. ACKNOWLEDGMENT

The author gratefully acknowledges the advice of Armando Guzmán on TW simulations and analyses.

XI. REFERENCES

- [1] IEEE Std C37.113, *IEEE Guide for Protective Relay Applications to Transmission Lines*.
- [2] *SEL-T400L Ultra-High-Speed Transmission Line Relay Traveling-Wave Fault Locator High-Resolution Event Recorder Instruction Manual*. Available: selinc.com.
- [3] S. Ward, "Comparison of Quadrilateral and Mho Distance Characteristic," proceedings of the 26th Annual Western Protective Relay Conference, Spokane, WA, October 1999.
- [4] G. Ziegler, *Numerical Distance Protection: Principles and Applications*, 4th ed., Publicis Corporate Publishing, Erlangen, Germany, 2011.
- [5] W. A. Elmore, *Protective Relaying Theory and Applications*, 2nd ed., Marcel Dekker, Inc., Monticello, NY, 2004.
- [6] S. Horowitz (ed.), *Protective Relaying for Power Systems*, IEEE Press, New York, NY, 1980.
- [7] Westinghouse Electric Corporation, *Applied Protective Relaying*, Newark, NJ, 1976.
- [8] P. K. Maezono, E. Altman, K. Brito, V. A. dos Santos Mello Maria, and F. Magrin, "Very High-Resistance Fault on a 525 kV Transmission Line – Case Study," proceedings of the 35th Annual Western Protective Relay Conference, Spokane, WA, October 2008.
- [9] F. Calero, A. Guzmán, and G. Benmouyal, "Adaptive Phase and Ground Quadrilateral Distance Elements," proceedings of the 36th Annual Western Protective Relay Conference, Spokane, WA, October 2009.
- [10] V. V. Terzija, R. Ciric, and H. Nouri, "Improved Fault Analysis Method Based on a New Arc Resistance Formula," *IEEE Transactions on Power Delivery*, Vol. 26, No. 1, January 2011, pp. 120–126.
- [11] A. R. van C. Warrington, "Reactance Relays Negligibly Affected by Arc Impedance," *Electrical World*, September 1931, pp. 502–505.
- [12] V. V. Terzija and H.-J. Koglin, "New Approach to Arc Resistance Calculation," proceedings of the IEEE Power Engineering Society Winter Meeting, January–February 2001.
- [13] Y. Goda, M. Iwata, K. Ikeda, and S. Tanaka, "Arc Voltage Characteristics of High Current Fault Arcs in Long Gaps," *IEEE Transactions on Power Delivery*, Vol. 15, No. 2, April 2000, pp. 791–795.
- [14] A. P. Strom, "Long 60-Cycle Arcs in Air," *Electrical Engineering*, Vol. 65, No. 3, March 1946, pp. 113–118.
- [15] J. L. Blackburn and T. J. Domin, *Protective Relaying: Principles, and Applications*, 3rd ed., CRC Press, LLC, Boca Raton, FL, 2007.
- [16] C. R. Mason, *The Art & Science of Protective Relaying*, John Wiley & Sons, Inc., New York, NY, 1956.
- [17] V. D. Andrade and E. Sorrentino, "Typical Expected Values of the Fault Resistance in Power Systems," proceedings of the IEEE/PES Transmission and Distribution Conference and Exposition, Sao Paulo, Brazil, November 2010.
- [18] Y. Gong, M. Mynam, A. Guzmán, G. Benmouyal, and B. Shulim, "Automated Fault Location System for Nonhomogeneous Transmission Networks," proceedings of the 65th Annual Conference for Protective Relay Engineers, College Station, TX, April 2012.
- [19] C. Bayliss and B. Hardy, *Transmission and Distribution Electrical Engineering*, 3rd ed., Elsevier Ltd., Burlington, MA, 2007.
- [20] H. H. Farr, *Transmission Line Design Manual*, United States Department of the Interior Water and Power Resources Service, Denver, CO, 1980.
- [21] G. Swift, D. Fedirchuk, and T. Ernst, "Arcing Fault 'Resistance' (It Isn't)," proceedings of the 6th Annual Georgia Tech Fault and Disturbance Analysis Conference, Atlanta, GA, May 2003.
- [22] Alstom Grid, *Network Protection & Automation Guide*, 2011.
- [23] Rural Utilities Service, *Design Guide for Rural Substations*, RUS Bulletin 1724E-300, United States Department of Agriculture, June 2001.
- [24] J. Berdy and K. Winick, "Application Guide for the Use of Distance Relays," General Electric Application Guide (GER-3199).
- [25] IEC 61936-1, *Power Installations Exceeding 1 kV a.c.*, 2014.
- [26] National Grid Technical Specification, *Substations*, TS 2.01 Part 1 (RES), Issue 1, October 2014. Available: nationalgrid.com.
- [27] S. Kaiser, "Different Representations of the Earth Impedance Matching in Distance Protection Relays, or What Impedance Does a Digital Distance Protection Relay Measure?" proceedings of theOMICRON User Conference, Germany, 2004.
- [28] E. O. Schweitzer, III, and J. Roberts, "Distance Relay Element Design," proceedings of the 19th Annual Western Protective Relay Conference, October 1992.
- [29] J. Roberts, A. Guzmán, and E. O. Schweitzer, III, "Z = V/I Does Not Make a Distance Relay," proceedings of the 20th Annual Western Protective Relay Conference, Spokane, WA, October 1993.
- [30] A. Rangel and K. Zimmerman, "Testing the SEL-421-4-5 Quadrilateral Phase Element for a Balanced Three-Phase Fault," SEL Application Guide (AG2014-08), 2014. Available: selinc.com.
- [31] E. O. Schweitzer, III, "New Developments in Distance Relay Polarization and Fault Type Selection," proceedings of the 16th Annual Western Protective Relay Conference, Spokane, WA, October 1989.
- [32] F. Calero, "Distance Elements: Linking Theory With Testing," proceedings of the 35th Annual Western Protective Relay Conference, Spokane, WA, October 2008.
- [33] G. E. Alexander, J. G. Andrichak, and W. Z. Tyska, "Relaying Short Lines," General Electric Application Guide (GER-3735).
- [34] *SEL-311C-1 Transmission Protection System Instruction Manual*. Available: selinc.com.
- [35] P. G. Mysore and A. Mulawarman, "Do We Have to Reduce Zone 1 Reach Solely Based on System Impedance Ratio – SIR?" proceedings of the 54th Annual Minnesota Power Systems Conference, Saint Paul, MN, November 2018.

- [36] M. J. Thompson and A. Somani, "A Tutorial on Calculating Source Impedance Ratios for Determining Line Length," proceedings of the 41st Annual Western Protective Relay Conference, Spokane, WA, October 2014.
- [37] *SEL-411L Advanced Line Differential Protection, Automation, and Control System Instruction Manual*. Available: selinc.com.
- [38] B. Kasztenny, "Settings Considerations for Distance Elements in Line Protection Applications," proceedings of the 74th Annual Conference for Protective Relay Engineers, March 2021.
- [39] D. Hou and J. Roberts, "Capacitive Voltage Transformers: Transient Overreach Concerns and Solutions for Distance Relaying," proceedings of the 22nd Annual Western Protective Relay Conference, Spokane, WA, October 1995.
- [40] D. Costello and K. Zimmerman, "CVT Transients Revisited – Distance, Directional Overcurrent, and Communications-Assisted Tripping Concerns," proceedings of the 65th Annual Conference for Protective Relay Engineers, College Station, TX, April 2012.
- [41] E. O. Schweitzer, III, K. Behrendt, and T. Lee, "Digital Communications for Power System Protection: Security, Availability, and Speed," proceedings of the 25th Annual Western Protective Relay Conference, Spokane, WA, October 1998.
- [42] ABB, *Type KD-10 and KD-11 Compensator Distance Relay, Instruction Leaflet 41-490J*, November 1999. Available: new.abb.com.
- [43] J. Roberts, E. O. Schweitzer, III, R. Arora, and E. Poggi, "Limits to the Sensitivity of Ground Directional and Distance Protection," proceedings of the 22nd Annual Western Protective Relay Conference, Spokane, WA, October 1995.
- [44] D. D. Fentie, "Understanding the Dynamic Mho Distance Characteristic," proceedings of the 42nd Annual Western Protective Relay Conference, Spokane, WA, October 2015.
- [45] The Alberta Electric System Operator (AESO), "Section 502.3 – Interconnected Electric System Protection Requirements," *ISO Rules, Part 500 Facilities, Division 502 Technical Requirements*. Available: aeso.ca.
- [46] H. J. Altuve, K. Zimmerman, and D. Tziouvaras, "Maximizing Line Protection Reliability, Speed, and Security," proceedings of the 42nd Annual Western Protective Relay Conference, Spokane, WA, October 2015.
- [47] *SEL-3031 Serial Radio Transceiver Instruction Manual*. Available: selinc.com.
- [48] D. A. Tziouvaras, H. J. Altuve, and F. Calero, "Protecting Mutually Coupled Transmission Lines: Challenges and Solutions," proceedings of the 40th Annual Western Protective Relay Conference, Spokane, WA, October 2013.
- [49] K. Zimmerman and D. Costello, "Fundamentals and Improvements for Directional Relays," proceedings of the 63rd Annual Conference for Protective Relay Engineers, College Station, TX, March 2010.
- [50] J. Mooney and J. Peer, "Application Guidelines for Ground Fault Protection," proceedings of the 24th Annual Western Protective Relay Conference, Spokane, WA, October 1997.
- [51] E. O. Schweitzer, III, and J. J. Kumm, "Statistical Comparison and Evaluation of Pilot Protection Schemes," proceedings of the 23rd Annual Western Protective Relay Conference, Spokane, WA, October 1996.
- [52] E. O. Schweitzer, III, and D. Hou, "Filtering for Protective Relays," proceedings of the 19th Annual Western Protective Relay Conference, Spokane, WA, October 1992.
- [53] G. Benmouyal and S. E. Zocholl, "The Impact of High Fault Current and CT Rating Limits on Overcurrent Protection," proceedings of the 29th Annual Western Protective Relay Conference, Spokane, WA, October 2002.
- [54] D. A. Tziouvaras, H. Altuve, G. Benmouyal, and J. Roberts, "Line Differential Protection With an Enhanced Characteristic," proceedings of the 3rd Mediterranean Conference on Power Generation, Transmission, Distribution, and Energy Conversion, Athens, Greece, November 2002.
- [55] B. Kasztenny, G. Benmouyal, H. J. Altuve, and N. Fischer, "Tutorial on Operating Characteristics of Microprocessor-Based Multiterminal Line Current Differential Relays," proceedings of the 38th Annual Western Protective Relay Conference, Spokane, WA, October 2011.
- [56] H. Miller, J. Burger, N. Fischer, and B. Kasztenny, "Modern Line Current Differential Protection Solutions," proceedings of the 36th Annual Western Protective Relay Conference, Spokane, WA, October 2009.
- [57] Y. Xue, B. Kasztenny, D. Taylor, and Y. Xia, "Series Compensation, Power Swings, and Inverter-Based Sources and Their Impact on Line Current Differential Protection," proceedings of the 66th Annual Conference for Protective Relay Engineers, College Station, TX, April 2013.
- [58] H. J. Altuve, J. B. Mooney, and G. E. Alexander, "Advances in Series-Compensated Line Protection," proceedings of the 35th Annual Western Protective Relay Conference, Spokane, WA, October 2008.
- [59] G. Benmouyal and J. Roberts, "Superimposed Quantities: Their True Nature and Application in Relays," proceedings of the 26th Annual Western Protective Relay Conference, Spokane, WA, October 1999.
- [60] E. O. Schweitzer, III, B. Kasztenny, and M. V. Mynam, "Performance of Time-Domain Line Protection Elements on Real-World Faults," proceedings of the 42nd Annual Western Protective Relay Conference, Spokane, WA, October 2015.
- [61] E. O. Schweitzer, III, B. Kasztenny, A. Guzmán, V. Skendzic, and M. V. Mynam, "Speed of Line Protection – Can We Break Free of Phasor Limitations?" proceedings of the 41st Annual Western Protective Relay Conference, Spokane, WA, October 2014.
- [62] E. O. Schweitzer, III, A. Guzmán, M. V. Mynam, V. Skendzic, B. Kasztenny, and S. Marx, "Locating Faults by the Traveling Waves They Launch," proceedings of the 40th Annual Western Protective Relay Conference, Spokane, WA, October 2013.
- [63] B. Kasztenny, M. V. Mynam, T. Joshi, and D. Holmbo, "Preventing Line Faults With Continuous Monitoring Based on Current Traveling Waves," proceedings of the 15th International Conference on Developments in Power System Protection, Liverpool, United Kingdom, March 2020.
- [64] A. Guzmán, B. Kasztenny, Y. Tong, and M. V. Mynam, "Accurate and Economical Traveling-Wave Fault Locating Without Communications," proceedings of the 44th Annual Western Protective Relay Conference, Spokane, WA, October 2017.
- [65] T. Hensler, C. Pritchard, N. Fischer, and B. Kasztenny, "Testing Superimposed-Component and Traveling-Wave Line Protection," proceedings of the 44th Annual Western Protective Relay Conference, Spokane, WA, October 2017.
- [66] A. Guzmán, G. Smelich, Z. Sheffield, and D. Taylor, "Testing Traveling-Wave Line Protection and Fault Locators," proceedings of the 14th International Conference on Developments in Power System Protection, Belfast, United Kingdom, March 2018.

XII. BIOGRAPHY

Donald D. Fentie received his B.Sc. degrees in Electrical Engineering and Computer Science in 2006 and his M.Sc. degree in Electrical Engineering in 2010 from the University of Saskatchewan. Donald worked for a company formerly known as Magna Electric Corporation as a protection engineer and field engineer in Saskatoon, Saskatchewan, from 2006 to 2010. He joined Schweitzer Engineering Laboratories, Inc. (SEL) in 2010 and is currently an application protection engineer in Calgary, Alberta. He is an IEEE member and is registered as a professional engineer in the province of Alberta.